DOI: 10.1021/ic100358m

Inorganic Chemistry
Article

Ruthenium Complexes with Cooperative PNP-Pincer Amine, Amido, Imine, and Enamido Ligands: Facile Ligand Backbone Functionalization Processes

Anja Friedrich, Markus Drees, Martina Käss, Eberhardt Herdtweck, and Sven Schneider*

Technische Universität München, Department Chemie, Lichtenbergstr. 4, 85747 Garching b, München, Germany

Received February 22, 2010

The quantitative formation of enamido complex [Ru(H)PMe_3(PNP′)] (**3**; PNP′ = N($CHCHP^iPr_2$)($CH_2CH_2P^iPr_2$)) from the reaction of [$RuCl_2PMe_3$(*H*PNP)] (**5**; *H*PNP = HN($CH_2CH_2P^iPr_2)_2$) with an excess of base (KO*t*Bu) can be explained by β-hydride migration from an intermediate amido complex [RuClPMe_3(PNP)] (**6**; PNP = N($CH_2CH_2P^iPr_2)_2$). Resulting imine complex [RuCl(H)PMe_3(PNP*)] (**7**; PNP* = N($CHCH_2P^iPr_2$)($CH_2CH_2P^iPr_2$)) could be independently synthesized and gives **3** with KO*t*Bu. A computational examination of the reversible double H_2 addition and elimination equilibria of enamide **3**, amido complex [Ru(H)PMe_3(PNP)] (**1**), and amine complex [$Ru(H)_2PMe_3$(*H*PNP)] (**2**) explains why [$Ru(H)_2PMe_3$(PNP*)] (**8**) is not observed experimentally. The distinctly different molecular and electronic structures of related complexes **1** and **3**, which feature a Y-shaped distorted trigonal-bipyramid (Y-TBP) for amide **1** but T-shaped TBP for enamide **3**, respectively, can be attributed to considerably reduced N→M π-donation for the PNP′ ligand due to delocalization of the *N*-lone pair into the unsaturated pincer backbone. The resulting low-lying LUMO of **3** explains its Lewis-acidic behavior, as documented by the formation of octahedral complex [RuH(PMe_3)$_2$(PNP′)] (**14**) upon the addition of PMe_3. In comparison, the reaction of **1** with PMe_3 gives a mixture of **2** and **14** via a base-assisted hydrogen elimination pathway. On the other hand, with electrophiles, such as MeOTf, predominant *N*-methylation is observed for both **1** and **3**, producing [RuH(OTf)PMe_3(*Me*PNP)] (**11**) and [RuH(OTf)-PMe_3(*Me*PNP′)] (**12**), respectively. This reactivity of **3** contrasts with pyridine-based cooperative pincer analogues and can be attributed to the high flexibility of the aliphatic PNP′ pincer ligand. The structural and reactivity patterns place this novel ligand between the parent PNP and aromatic pincer ligands.

Introduction

Terminal π-donating ligands, such as amides, were for a long time considered unsuitable for late transition metals owing to the *hard* ligand and *soft* metal mismatch. In fact, the high electron count of metal centers with $d^n \geq d^6$ results in distinctly different properties as compared with electron poor metal amido complexes,[1] and repulsive filled−filled π-interactions of the nitrogen free electron pair with metal d electrons strongly determine the reactivity of this compound class.[2,3] Owing to the pronounced ligand nitrogen centered reactivity, such as the high basicity and nucleophilicity,[4] late transition metal amido complexes are ideal compounds to examine metal−ligand cooperativity. Cooperating ligands are directly involved in reversible chemical transformations of metal complexes. This concept has recently attracted considerable interest to accelerate absolute and relative rates of bond activation reactions aimed at improving activity and selectivity in catalysis.[5] As a prominent example, Noyori and Ohkuma introduced ruthenium amido catalysts for the hydrogenation and transfer hydrogenation of carbonyl groups, for which a bifunctional mechanism has been proposed with

*To whom correspondence should be addressed. E-mail: sven.schneider@ch.tum.de.

(1) (a) Bryndza, H. E.; Tam, W. *Chem. Rev.* **1988**, *88*, 1163–1188. (b) Fryzuk, M. D.; Montgomery, C. D. *Coord. Chem. Rev.* **1989**, *95*, 1–40. (c) Roundhill, D. M. *Chem. Rev.* **1992**, *92*, 1–27. (d) Fulton, J. R.; Holland, A. W.; Fox, D. J.; Bergman, R. G. *Acc. Chem. Res.* **2002**, *35*, 44–56. (e) Gunnoe, T. B. *Eur. J. Inorg. Chem.* **2007**, 1185–1203.

(2) Caulton, K. G. *New J. Chem.* **1994**, *18*, 25–41.

(3) Alternatively, the nitrogen centered nucleophilicity has been attributed to the high M−N σ-bond polarity: Holland, P. L.; Andersen, R. A.; Bergman, R. G. *Comments Inorg. Chem.* **1999**, *21*, 115–129.

(4) (a) Park, S.; Rheingold, A. L.; Roundhill, D. M. *Organometallics* **1991**, *10*, 615–623. (b) Fulton, J. R.; Bouwkamp, M. W.; Bergman, R. G. *J. Am. Chem. Soc.* **2000**, *122*, 8799–8800. (c) Büttner, T.; Breher, F.; Grützmacher, H. *Chem. Commun.* **2004**, 2820–2821. (d) Maire, P.; Breher, F.; Schönberg, H.; Grützmacher, H. *Organometallics* **2005**, *24*, 3207–3218. (e) Büttner, T.; Geier, J.; Frison, G.; Harmer, J.; Calle, C.; Schweiger, A.; Schönberg, H.; Grützmacher, H. *Science* **2005**, *307*, 235–238. (f) Marziale, A. N.; Herdtweck, E.; Eppinger, J.; Schneider, S. *Inorg. Chem.* **2009**, *48*, 3699–3709. (g) Askevold, B.; Friedrich, A.; Buchner, M. R.; Marziale, A. N.; Herdtweck, E.; Schneider, S. Manuscript in preparation.

(5) Some recent reviews: (a) Rowlands, G. J. *Tetrahedron* **2001**, *57*, 1865–1882. (b) Grützmacher, H. *Angew. Chem.* **2008**, *120*, 1838–1842. Grützmacher, H. *Angew. Chem., Int. Ed.* **2008**, *47*, 1814−1818. (c) Grotjahn, D. B. *Dalton Trans.* **2008**, 6497–6508. (d) Park, Y. J.; Park, J.-W.; Jun, C.-H. *Acc. Chem. Res.* **2008**, *41*, 222–234. (e) van der Vlugt, J. I.; Reek, J. N. H. *Angew. Chem.* **2009**, *121*, 8990–9004. van der Vlugt, J. I.; Reek, J. N. H. *Angew. Chem., Int. Ed.* **2009**, *48*, 8832−8846.

Published on Web 05/20/2010

concerted transfer of a nitrogen bound proton and a hydride to the substrate.[6] Subsequent H_2 activation is accomplished by direct or acid catalyzed proton transfer from a dihydrogen ligand to the amido moiety.[7] More recently, bifunctional ruthenium amido catalysts were also successfully applied in the reverse reaction: the acceptor-less dehydrogenation of organic and inorganic substrates, such as alcohols, formic acid, or borane amines.[8−10] These reactions are of great interest for applications both in synthesis and in hydrogen storage.[11]

As a fundamental reactivity of late transition metal amido complexes, such compounds bearing β-hydrogen atoms typically suffer from low thermodynamic stability, owing to decomposition toward metal hydrides by imine extrusion.[1a,b,12] Accordingly, ruthenium imine complexes have been identified as deactivation products from Noyori-type hydrogenation catalysts.[13] Furthermore, the reverse reaction, i.e., hydride migration to a metal bound imine, defines an important elementary step in catalytic imine hydrogenation.[6b] However, despite the high relevance of frequently observed β-hydride elimination in late transition metal amido chemistry, only few mechanistic studies have been published, contrasting sharply with β-H elimination in alkyl complexes.[14,15]

We have recently presented the use of amido complex [Ru(H)PMe_3(PNP)] (**1**; PNP = $N(CH_2CH_2P^iPr_2)_2$) as a highly efficient catalyst for borane−amine dehydrogenation.[10b,c]

Scheme 1. H_2 Elimination/Addition Reactions of Amine, Amido, and Enamido Complexes **2**, **1**, and **3**

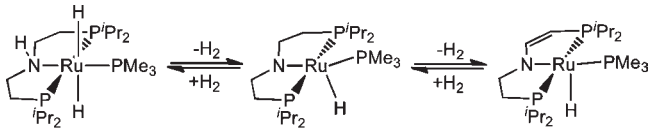

Furthermore, iridium and ruthenium complexes with amine ligand *H*PNP ($HN(CH_2CH_2P^iPr_2)_2$) are highly active catalysts for the hydrogenation and transfer hydrogenation of $R_2C{=}E$ (E = O, NR) double bonds.[16] Complex **1** can be synthesized from amine complex [Ru(H)$_2$$PMe_3$(*H*PNP)] (**2**) upon H_2 elimination,[10b,7c] and **2** results from the reaction of enamide [Ru(H)PMe_3(PNP′)] (**3**; PNP′ = $N(CHCHP^iPr_2)(CH_2CH_2P^iPr_2)$) with excess H_2. Furthermore, it was shown for the double hydrogen addition and elimination equilibria of **1**, **2**, and **3** to be reversible (Scheme 1), demonstrating the 2-fold *cooperativity* of the pincer ligand. While the oxidation of amine ligands with hydrogen acceptors (e.g., O_2) or electrochemical oxidation of amines are well studied, acceptor-less dehydrogenation remains scarcely investigated.[17] Therefore, we were interested in elucidating the mechanism for the formation of **3**.

In this paper, we report a combined experimental and computational study to clarify the C−H activation processes in the PNP pincer backbone. These results can serve as a model for imine hydrogenation and, more specifically, comprise valuable information for the design of future cooperative ligands in catalysis. We will first present a plausible mechanism for the pincer backbone C−H activation processes. Since the new enamido type PNP′ ligand of **3** is on first sight similar to the parent PNP amido ligand, further emphasis will be put into the examination of the PNP− and PNP′−d^6 ruthenium complex electronic structures (Figure 1). This comparison reveals that the reactivity, particularly with nucleophiles, can be controlled by ligand backbone de/hydrogenation as a consequence of tunable π donation of the cooperating ligand.

Experimental Section

Materials and Methods. All experiments were carried out under an atmosphere of argon using Schlenk and glovebox techniques. Benzene and THF were dried over Na/benzophenone, distilled under argon, and deoxygenated prior to use. Pentane was dried and deoxygenized by passing through columns packed with activated alumina and Q5, respectively. Deuterated solvents were dried by distillation from a Na/K alloy (C_6D_6 and d^8-THF) and deoxygenated by three freeze−pump−thaw cycles. KO^{t}Bu was purchased from VWR and sublimed prior to use. A 1 M HCl solution in Et_2O (Aldrich), $LiBHEt_3$ (1 M solution in THF) (ACROS), H_2 (5.0, Westfalen), and D_2 (99.96, ISOTEC) were used as purchased. Complexes **1**, **3**, and **10** were prepared as reported earlier.[7c,10b]

Analytical Methods. Elemental analyses were obtained from the Microanalytical Laboratory of Technische Universität München. The IR spectra were recorded on a Jasco FT/IR-460 PLUS spectrometer as nujol mulls between KBr plates. NMR spectra were recorded on Jeol Lambda 400 and Bruker Avance III 400 NMR spectrometers at room temperature and were calibrated

(6) (a) Noyori, R.; Ohkuma, T. *Angew. Chem.* **2001**, *113*, 40–75. *Angew. Chem., Int. Ed.* **2001**, *40*, 40-73. (b) Clapham, S. E.; Hadzovic, A.; Morris, R. H. *Coord. Chem. Rev.* **2004**, *248*, 2201–2237. (c) Muñiz, K. *Angew. Chem.* **2005**, *117*, 6780–6785. Muñiz, K. *Angew. Chem., Int. Ed.* **2005**, *44*, 6622−6627. (d) Samec, J. S. M.; Bäckvall, J.-E.; Andersson, P. G.; Brandt, P. *Chem. Soc. Rev.* **2006**, *35*, 237–248.

(7) (a) Abdur-Rashid, K.; Clapham, S. E.; Hadzovic, A.; Harvey, J. N.; Lough, A. J.; Morris, R. H. *J. Am. Chem. Soc.* **2002**, *124*, 15104–15118. (b) Sandoval, C. A.; Ohkuma, T.; Muñiz, K.; Noyori, R. *J. Am. Chem. Soc.* **2003**, *125*, 13490–13503. (c) Friedrich, A.; Drees, M.; Schmedt auf der Günne, J.; Schneider, S. *J. Am. Chem. Soc.* **2009**, *131*, 17552–17553.

(8) Zhao, J.; Hartwig, J. F. *Organometallics* **2005**, *24*, 2441–2446.

(9) Morris, D. J.; Clarkson, G. J.; Wills, M. *Organometallics* **2009**, *28*, 4133–4140.

(10) (a) Blaquiere, N.; Diallo-Garcia, S.; Gorelsky, S. I.; Black, D. A.; Fagnou, K. *J. Am. Chem. Soc.* **2008**, *130*, 14034–14035. (b) Käss, M.; Friedrich, A.; Drees, M.; Schneider, S. *Angew. Chem.* **2009**, *121*, 922–924. *Angew. Chem., Int. Ed.* **2009**, *48*, 905−907. (c) Friedrich, A.; Drees, M.; Schneider, S. *Chem.—Eur. J.* **2009**, *15*, 10339–10342.

(11) (a) Hamid, M. H. S. A.; Slatford, P. A.; Williams, J. M. J. *Adv. Synth. Catal.* **2007**, *349*, 1555–1575. (b) Boddien, A.; Loges, B.; Junge, H.; Beller, M. *ChemSusChem* **2008**, *1*, 751–758. (c) Bower, J. F.; Kim, I. S.; Patman, R. L.; Krische, M. J. *Angew. Chem.* **2009**, *121*, 36–48. Bower, J. F.; Kim, I. S.; Patman, R. L.; Krische, M. J. *Angew. Chem., Int. Ed.* **2009**, *48*, 34−46. (d) Friedrich, A.; Schneider, S. *ChemCatChem* **2009**, *1*, 72–73. (e) Johnson, T. C.; Morris, D. J.; Wills, M. *Chem. Soc. Rev.* **2010**, *39*, 81–88.

(12) (a) Diamond, S. E.; Mares, F. *J. Organomet. Chem.* **1977**, *142*, C55–C57. (b) Hartwig, J. F. *J. Am. Chem. Soc.* **1996**, *118*, 7010–7011. (c) Hartwig, J. F.; Richards, S.; Barañano, D.; Paul, F. *J. Am. Chem. Soc.* **1996**, *118*, 3626–3633. (d) Wagaw, S.; Rennels, R. A.; Buchwald, S. L. *J. Am. Chem. Soc.* **1997**, *119*, 8451–8458.

(13) Abbel, R.; Abdur-Rashid, K.; Faatz, M.; Hadzovic, A.; Lough, A. J.; Morris, R. H. *J. Am. Chem. Soc.* **2005**, *127*, 1870–1882.

(14) (a) Mayer, J. M.; Curtis, C. J.; Bercaw, J. E. *J. Am. Chem. Soc.* **1983**, *105*, 2651–2660. (b) Hartwig, J. F. *J. Am. Chem. Soc.* **1996**, *118*, 7010–7011. (c) Tsai, Y.-C.; Johnson, M. J. A.; Mindiola, D. J.; Cummins, C. C. *J. Am. Chem. Soc.* **1999**, *121*, 10426–10427. (d) Zhao, J.; Hesslink, H.; Hartwig, J. F. *J. Am. Chem. Soc.* **2001**, *123*, 7220–7227. (e) Zhao, P.; Hartwig, J. F. *J. Am. Chem. Soc.* **2005**, *127*, 12066–12073. (f) Matas, I.; Campora, J.; Palma, P.; Alvarez, E. *Organometallics* **2009**, *28*, 6515–6523.

(15) (a) Collman, J. P.; Hegedus, L. S.; Norton, J. R.; Finke, R. G. In *Principles and Applications of Organotransition Metal Chemistry*; University Science Books: Sausalito, CA, 1987. (b) Crabtree, R. H. In *The Organometallic Chemistry of the Transition Metals*, 3rd ed.; Wiley-Interscience: New York, 2001. (c) Niu, S.; Hall, M. B. *Chem. Rev.* **2000**, *100*, 353–405.

(16) (a) Clarke, Z. E.; Maragh, P. T.; Dasgupta, T. P.; Gusev, D. G.; Lough, A. J.; Abdur-Rashid, K. *Organometallics* **2006**, *25*, 4113–4117. (b) Amoroso, D.; Graham, T. W.; Guo, R.; Tsang, C.-W.; Abdur-Rashid, K. *Aldrichim. Acta* **2008**, *41*, 15–26. (c) Chen, X.; Jia, W.; Guo, R.; Graham, T. W.; Gullons, M. A.; Abdur-Rashid, K. *Dalton Trans.* **2009**, 1407–1410.

(17) Keene, R. F. *Coord. Chem. Rev.* **1999**, *187*, 121–149.

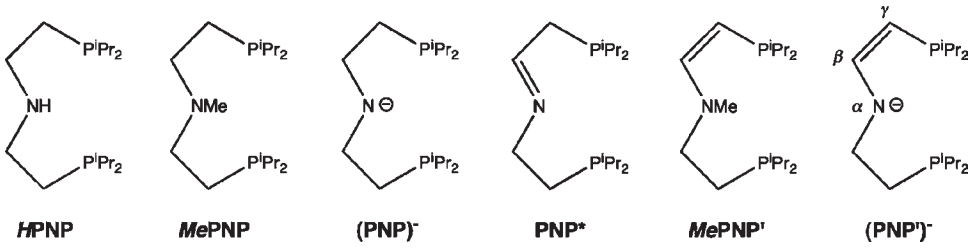

Figure 1. Nomenclature for the PNP pincer ligands used throughout this paper.

to the residual proton resonance and the natural abundance ^{13}C resonance of the solvent (C_6D_6, $\delta_H = 7.16$ and $\delta_C = 128.06$ ppm; d_8-THF, $\delta_H = 1.72$ and 3.57 ppm, $\delta_C = 25.3$ and 67.4 ppm). ^{31}P NMR chemical shifts are reported relative to external phosphoric acid (δ 0.0 ppm). Signal multiplicities are abbreviated as s (singlet), d (doublet), t (triplet), q (quartet), sept (septet), m (multiplet), and br (broad).

Syntheses. **[RuHCl(PMe$_3$)(PNP*)] (7).** Complex **3** (0.127 g; 0.264 mmol) is dissolved in THF (10 mL), and a solution of HCl in Et_2O (1 M; 264 μL; 0.264 mmol) is added via syringe at room temperature. The color immediately changes to brownish yellow. After 5 min at room temperature, the solvent is evaporated *in vacuo* to give a yellow-brown oil. The residue is dissolved in THF, and pentane (5 mL) is added. After crystallization overnight at −35 °C, the precipitate is filtered off to give **7** as a yellow solid. Yield: 0.068 g (0.132 mmol; 50%). Small amounts of [RuHCl(PMe$_3$)(PNP^H)] (< 2%) were detected by ^1H and ^{31}P NMR. Anal. Calcd for $C_{19}H_{45}ClNP_3Ru$ (517.02): C, 44.14; H, 8.77; N, 2.71. Found: C, 45.05; H, 9.34; N, 2.53. IR (cm^{-1}): ν 1957 (s, Ru−H), 1616 (m, C=N). NMR (C_6D_6, r.t., [ppm]) ^1H NMR (399.8 MHz): δ −19.20 (dt, $^2J_{HP}$ = 26.5 Hz, $^2J_{HP}$ = 22.2 Hz, 1H, Ru-*H*), 0.79 (dd, $^3J_{HP}$ = 11.8 Hz, $^3J_{HH}$ = 6.7 Hz, 3H, CHC*H*$_3$), 0.96 (dd, $^3J_{HP}$ = 11.6 Hz, $^3J_{HH}$ = 6.9 Hz, 3H, CHC*H*$_3$), 1.02 (dd, $^3J_{HP}$ = 15.7 Hz, $^3J_{HH}$ = 7.6 Hz, 3H, CHC*H*$_3$), 1.07 (dd, $^3J_{HP}$ = 14.5 Hz, $^3J_{HH}$ = 6.9 Hz, 3H, CHC*H*$_3$), 1.11 (dd, $^3J_{HP}$ = 10.5 Hz, $^3J_{HH}$ = 7.1 Hz, 3H, CHC*H*$_3$), 1.23 (dd, $^3J_{HP}$ = 10.7 Hz, $^3J_{HH}$ = 7.0 Hz, 3H, CHC*H*$_3$), 1.42 (d, $^2J_{HP}$ = 7.8 Hz, 9H, P(C*H*$_3$)$_3$), 1.54 (dd, $^3J_{HP}$ = 13.3 Hz, $^3J_{HH}$ = 7.4 Hz, 3H, CHC*H*$_3$), 1.62 (dd, $^3J_{HP}$ = 14.3 Hz, $^3J_{HH}$ = 7.1 Hz, 3H, CHC*H*$_3$), 1.66−1.89 (m, 2H, C*H*(CH$_3$)$_2$ + 2H, PC*H*$_2$CH$_2$N), 1.96 (ddt, $^2J_{HP}$ = 17.9 Hz, $^3J_{HH}$ = 8.5 Hz, $^4J_{HP}$ = 2.5 Hz, 1H, PC*H*$_2$CHN), 2.14 (m, 1H, C*H*(CH$_3$)$_2$), 2.60−2.76 (m, 1H, C*H*(CH$_3$)$_2$ + 1H, PC*H*$_2$CHN), 3.11 (m, 1H, NC*H*$_2$), 3.62 (m, 1H, NC*H*$_2$), 7.30 (dd, $^3J_{HP}$ = 21.5 Hz, $^4J_{HP}$ = 3.8 Hz, 1H, N=C*H*). ^{13}C {^1H} NMR (100.6 MHz): δ 17.9 (s, CH*C*H$_3$), 18.3 (dd, $^2J_{CP}$ = 3.8 Hz, $^4J_{CP}$ = 1.8 Hz, CH*C*H$_3$), 18.8 (dd, $^2J_{CP}$ = 2.7 Hz, $^4J_{CP}$ = 1.9 Hz, CH*C*H$_3$), 19.0 (d, $^2J_{CP}$ = 6.5 Hz, CH*C*H$_3$), 19.1 (s, CH*C*H$_3$), 19.6 (d, $^2J_{CP}$ = 5.0 Hz, CH*C*H$_3$), 20.1 (d, $^2J_{CP}$ = 5.8 Hz, CH*C*H$_3$), 20.2 (d, $^2J_{CP}$ = 2.3 Hz, CH*C*H$_3$), 24.7 (dd, $^1J_{CP}$ = 14.6 Hz, $^3J_{CP}$ = 2.7 Hz, PCH$_2$CH$_2$N), 24.9 (dt, $^1J_{CP}$ = 24.6 Hz, $^3J_{CP}$ = 2.7 Hz, P(*C*H$_3$)$_3$), 26.2 (dd, $^1J_{CP}$ = 20.4 Hz, $^3J_{CP}$ = 1.5 Hz, *C*H(CH$_3$)$_2$), 26.4 (dd, $^1J_{CP}$ = 19.6 Hz, $^3J_{CP}$ = 1.1 Hz, *C*H(CH$_3$)$_2$), 27.0 (ddd, $^1J_{CP}$ = 8.1 Hz, $^3J_{CP}$ = 5.8 Hz, $^3J_{CP}$ = 1.2 Hz, *C*H(CH$_3$)$_2$), 27.5 (ddd, $^1J_{CP}$ = 7.7 Hz, $^3J_{CP}$ = 6.6 Hz, $^3J_{CP}$ = 1.2 Hz, *C*H(CH$_3$)$_2$), 35.1 (dd, $^1J_{CP}$ = 15.0 Hz, $^3J_{CP}$ = 4.2 Hz, PCH$_2$-CHN), 60.4 (dd, $^2J_{CP}$ = 6.5 Hz, $^3J_{CP}$ = 1.1 Hz, NCH$_2$), 163.2 (dd, $^2J_{CP}$ = 6.9 Hz, $^3J_{CP}$ = 1.9 Hz, N=*C*H). ^{31}P {^1H} NMR (161.8 MHz): δ 75.2 (dd, $^2J_{PP}$ = 30 Hz, $^2J_{PP}$ = 281 Hz, *P*^{i}Pr$_2$), 66.9 (dd, $^2J_{PP}$ = 30 Hz, $^2J_{PP}$ = 281 Hz, *P*^{i}Pr$_2$), 9.4 (t, $^2J_{PP}$ = 30 Hz, *P*(CH$_3$)$_3$). Assignments were confirmed by ^1H COSY, ^1H NOESY, $^1H-^{13}C$ HETCOR (Supporting Information), and ^{13}C {^1H} DEPT spectra.

[RuH(PMe$_3$)OTf(*Me*PNP')] (12). MeOTf (0.060 g; 0.366 mmol) is added dropwise to a vigorously stirred solution of **3** (154.0 mg; 0.320 mmol) in benzene (5 mL) at room temperature. The color immediately changes from deep green to brown and a small amount of pentane is added to precipitate some oily contents. After filtration, the solvent is removed *in vacuo* to give 0.192 g of the greenish brown raw product with 70% of **12** determined by ^{31}P NMR. The residue is washed with pentane (3 × 5 mL) and dried *in vacuo* to give **12** as an analytically pure pale yellow solid. Yield: 0.080 g (0.124 mmol; 39%). Anal. Calcd for $C_{21}H_{47}F_3NO_3P_3RuS$ (644.65): C, 39.13; H, 7.35; N, 2.17; F, 8.84; S, 4.97. Found: C, 38.76; H, 7.30; N, 2.11; F, 8.9; S, 4.82. IR (cm^{-1}): ν 2143 (s, Ru−H), 1639 (s, C=C). NMR (C_6D_6, r.t., [ppm]) ^1H NMR (399.8 MHz): δ −25.92 (q, $^2J_{HP}$ = 23.8 Hz, 1H, RuH), 0.76 (dd, $^3J_{HH}$ = 6.8 Hz, $^3J_{HP}$ = 11.7 Hz, 3H, CHC*H*$_3$), 0.85 (m, 6H, CHC*H*$_3$), 0.95 (dd, $^3J_{HH}$ = 7.1 Hz, $^3J_{HP}$ = 13.7 Hz, 3H, CHC*H*$_3$), 1.10 (dd, $^3J_{HH}$ = 6.6 Hz, $^3J_{HP}$ = 10.0 Hz, 3H, CHC*H*$_3$ + 1H, PC*H*$_2$), 1.18 (dd, $^3J_{HH}$ = 7.1 Hz, $^3J_{HP}$ = 12.0 Hz, 3H, CHC*H*$_3$), 1.40−1.52 (m, 6H, CHC*H*$_3$ + 1H, PC*H*$_2$), 1.49 (d, $^2J_{HP}$ = 8.5 Hz, 9H, P(C*H*$_3$)$_3$), 1.67−1.81 (m, 2H, C*H*(CH$_3$)$_2$ + 1H, NC*H*$_2$), 2.02 (dm, 1H, NC*H*$_2$), 2.15−2.25 (m, 2H, C*H*-(CH$_3$)$_2$), 2.28 (s, 3H, NC*H*$_3$), 5.22 (d, $^3J_{HH}$ = 6.1 Hz, 1H, PC*H*), 5.45 (ddt, $^3J_{HP}$ = 27.4 Hz, $^3J_{HH}/^4J_{HP}$ = 6.4 Hz, $^4J_{HP}$ = 1.7 Hz, 1H, NC*H*). ^{13}C {^1H} NMR (100.6 MHz): δ 17.9 (dd, $^2J_{CP}$ = 2.6 Hz, $^4J_{CP}$ = 1.5 Hz, CH*C*H$_3$), 18.2 (d, $^2J_{CP}$ = 0.7 Hz, CH*C*H$_3$), 18.6 (d, $^2J_{CP}$ = 0.9 Hz, CH*C*H$_3$), 18.8 (s, CH*C*H$_3$), 19.1 (d, $^2J_{CP}$ = 3.3 Hz, CH*C*H$_3$), 19.3 (d, $^2J_{CP}$ = 4.8 Hz, CH*C*H$_3$), 19.4 (s, CH*C*H$_3$), 19.5 (d, $^2J_{CP}$ = 1.4 Hz, CH*C*H$_3$), 22.4 (dt, $^1J_{CP}$ = 14.8 Hz, $^3J_{CP}$ = 0.9 Hz, PCH$_2$), 25.7 (dd, $^1J_{CP}$ = 24.4 Hz, $^3J_{CP}$ = 3.2 Hz, *C*H(CH$_3$)$_2$), 25.8 (dt, $^1J_{CP}$ = 26.8 Hz, $^3J_{CP}$ = 2.8 Hz, P(*C*H$_3$)$_3$), 27.2 (ddd, $^1J_{CP}$ = 18.6 Hz, $^3J_{CP}$ = 6.1 Hz, $^3J_{CP}$ = 1.4 Hz, *C*H(CH$_3$)$_2$), 27.2 (dt, $^1J_{CP}$ = 5.8 Hz, $^3J_{CP}$ = 1.3 Hz, *C*H(CH$_3$)$_2$), 28.9 (dd, $^1J_{CP}$ = 23.2 Hz, $^3J_{CP}$ = 2.6 Hz, *C*H(CH$_3$)$_2$), 46.7 (s, NC*H*$_3$), 63.2 (dt, $^2J_{CP}$ = 6.2 Hz, $^3J_{CP}$ = 1.1 Hz, NCH$_2$), 120.8 (q, $^1J_{CF}$ = 319.5 Hz, SO_3CF_3), 121.5 (ddd, $^1J_{CP}$ = 22.3 Hz, $^3J_{CP}$ = 3.1 Hz, $^3J_{CP}$ = 1.5 Hz, PCH), 157.5 (ddd, $^2J_{CP}$ = 11.1 Hz, $^3J_{CP}$ = 2.7 Hz, $^3J_{CP}$ = 1.1 Hz, NCH). ^{31}P {^1H} NMR (161.83 MHz): δ 60.7 (dd, $^2J_{PP}$ = 261.7 Hz, $^2J_{PP}$ = 30.7 Hz, CHP^{i}Pr$_2$), 57.5 (dd, $^2J_{PP}$ = 261.7 Hz, $^2J_{PP}$ = 30.7 Hz, CH$_2$P^{i}Pr$_2$), 14.0 (t, $^2J_{PP}$ = 30.7 Hz, *P*(CH$_3$)$_3$). ^{19}F NMR (376.17 MHz): δ −77.5 (s, SO_3CF_3). Assignments were confirmed by ^1H COSY, $^1H-^{13}C$ HMQC (Supporting Information), and ^1H {sel. ^{31}P} NMR spectra.

Reaction of 7 with KO^{t}Bu. Potassium *tert*-butoxide (0.004 g; 0.038 mmol) is added to a solution of **7** (0.020 g; 0.039 mmol) in 0.4 mL of THF in a *J-Young*-NMR tube. The suspension immediately changes the color to deep green, and **3** is observed as the only product by ^{31}P NMR.

Reaction of 7 with HCl. HCl in Et_2O (1 M; 42 μL; 0.042 mmol) is added to a solution of **7** (0.021 g; 0.041 mmol) in 0.4 mL of THF in a septum cap NMR tube. Complex **5** is exclusively observed by ^{31}P NMR.

Reaction of 7 with LiBHEt$_3$. The addition of $LiBHEt_3$ in THF (1 M; 10 μL; 0.010 mmol) to a solution of **7** (0.006 g; 0.012 mmol) in 0.4 mL of THF in a septum cap NMR tube results in a red suspension. Complex **1** is observed as the only product by ^{31}P NMR.

Reaction of 5 with LiBHEt$_3$. $LiBHEt_3$ in THF (1 M; 400 μL; 0.400 mmol; 18 equiv) is added to a solution of **5** (0.012 g; 0.022 mmol) in 0.4 mL of THF in a septum cap NMR tube. Complex **2** is observed as the product by ^{31}P NMR exclusively.

[RuH(PMe$_3$)$_2$(PNP')] (14) Method A. To a suspension of **5** (0.082 g; 0.148 mmol) and potassium *tert*-butoxide (0.059 g;

0.526 mmol; 3.6 equiv) in THF (10 mL) is added a solution of PMe_3 in THF (1 M; 160 μL; 0.160 mmol) via syringe at room temperature. The dark green color immediately changes to pale brown. After 5 min at room temperature, the solvent is evaporated *in vacuo* to give a pale brown solid. After extraction with pentane (10 mL), the filtrate is evaporated, and the residue is dried overnight, redissolved in pentane (10 mL), and filtrated again. Evaporation of the filtrate gives **14** as a pale brown solid. Yield: 0.071 g (0.128 mmol; 86%). Anal. Calcd for $C_{22}H_{53}NP_4Ru$ (556.63): C, 47.47; H, 9.60; N, 2.52. Found: C, 47.48; H, 9.72; N, 2.50. IR (cm^{-1}) ν 1968 (s, Ru−H). NMR (C_6D_6, r.t., [ppm]). ^1H NMR (399.8 MHz): δ −10.30 (dq, $^2J_{HP}$ = 87.7 Hz, $^2J_{HP}$ = 26.2 Hz, 1H, Ru-*H*), 1.00−1.10 (m, 9H, CHCH_3), 1.14−1.19 (m, 3H, CHCH_3), 1.16 (d, $^2J_{HP}$ = 4.9 Hz, 9H, P(CH_3)$_3$), 1.27 (d, $^2J_{HP}$ = 6.8 Hz, 9H, P(CH_3)$_3$), 1.31−1.46 (m, 12H, CHCH_3), 1.46−1.52 (m, 1H, PCH_2), 1.58−1.67 (m, 1H, PCH_2), 1.88 (dsept, $^2J_{HP}$ = 2.4 Hz, $^3J_{HH}$ = 7.2 Hz, 2H, C*H*(CH$_3$)$_2$), 2.08 (sept, $^3J_{HH}$ = 6.7 Hz, 1H, C*H*(CH$_3$)$_2$), 2.27 (dsept, $^2J_{HP}$ = 3.4 Hz, $^3J_{HH}$ = 7.2 Hz, 1H, C*H*(CH$_3$)$_2$), 3.10−3.21 (m, 2H, NCH_2), 3.56 (d, $^3J_{HH}$ = 4.8 Hz, 1H, PC*H*), 7.28 (ddt, $^3J_{HP}$ = 38.2 Hz, $^3J_{HH}$/$^4J_{HP}$ = 4.9 Hz, $^4J_{HP}$ = 1.4 Hz, 1H, NC*H*). ^{13}C-{^1H} NMR (100.6 MHz): δ 19.2 (s, CH*C*H$_3$), 19.3 (s, CH*C*H$_3$), 19.8 (s, CH*C*H$_3$), 19.9 (s, CH*C*H$_3$), 20.2 (s, CH*C*H$_3$), 20.6 (d, $^2J_{CP}$ = 4.1 Hz, CH*C*H$_3$), 20.9 (s, CH*C*H$_3$), 22.1 (d, $^2J_{CP}$ = 4.9 Hz, CH*C*H$_3$), 23.0 (d, $^1J_{CP}$ = 13.5 Hz, P(*C*H$_3$)$_3$), 27.9 (ddd, $^1J_{CP}$ = 24.2 Hz, $^3J_{CP}$ = 9.4 Hz, $^3J_{CP}$ = 2.6 Hz, *C*H(CH$_3$)$_2$), 28.5 (d, $^1J_{CP}$ = 22.3 Hz, P(*C*H$_3$)$_3$ + superimposed *C*H(CH$_3$)$_2$), 29.1 (ddd, $^1J_{CP}$ = 25.7 Hz, $^3J_{CP}$ = 5.7 Hz, $^3J_{CP}$ = 1.9 Hz, *C*H(CH$_3$)$_2$), 29.7 (d, $^1J_{CP}$ = 16.9 Hz, P*C*H$_2$), 30.6 (dt, $^1J_{CP}$ = 13.1 Hz, $^3J_{CP}$ = 5.8 Hz, *C*H(CH$_3$)$_2$), 53.6 (dd, $^2J_{CP}$ = 5.3 Hz, $^3J_{CP}$ = 2.1 Hz, N*C*H$_2$), 66.3 (dd, $^1J_{CP}$ = 40.3 Hz, $^3J_{CP}$ = 5.2 Hz, P*C*H), 161.9 (d, $^2J_{CP}$ = 20.9 Hz, N*C*H). ^{31}P {^1H} NMR (161.8 MHz): δ 72.3 (ddd, $^2J_{PP}$ = 224.3 Hz, $^2J_{PP}$ = 24.8 Hz, $^2J_{PP}$ = 17.8 Hz, P^iPr$_2$), 67.2 (ddd, $^2J_{PP}$ = 224.3 Hz, $^2J_{PP}$ = 24.8 Hz, $^2J_{PP}$ = 17.8 Hz, P^iPr$_2$), 3.2 (q, $^2J_{PP}$ = 24.8 Hz, N−Ru-*P*Me$_3$), −19.6 (q, $^2J_{PP}$ = 17.8 Hz, H−Ru-*P*Me$_3$). Assignments were confirmed by ^1H COSY and $^1H-^{13}C$ HMQC NMR spectra (Supporting Information).

Method B. Complex **3** (0.095 g; 0.198 mmol) is dissolved in THF (10 mL), and a solution of PMe_3 in THF (1 M; 200 μL; 0.200 mmol) is added via syringe at room temperature. The color immediately changes from dark green to pale orange. After 10 min at room temperature, the solvent is evaporated *in vacuo* to give a pale brown solid. Yield: 0.109 g (0.196 mmol; 99%). The spectroscopic data (^1H NMR, ^{13}C NMR, ^{31}P NMR) are identical with those of Method A.

Reaction of 1 with PMe_3. PMe_3 in THF (1 M; 60 μL; 0.060 mmol) is added to a solution of **1** (0.010 g; 0.021 mmol) in 0.4 mL of d_8-THF in a septum-cap NMR tube. The reaction is monitored by ^{31}P and ^1H NMR at room temperature. An increase of an equimolar mixture of **2** and **14** is detected until complete conversion of **1** after 24 h.

H/D Exchange Studies. A solution of **1** (11.2 mg; 23.2 μmol; 52 mM) in d_8-THF and benzene as an internal standard was frozen in a *J-Young*-NMR tube, evacuated, and backfilled with D_2 (1 bar). After quantitative formation of [Ru(D)$_2$PMe$_3$-{DN(CH$_2$CH$_2$P^{i}Pr$_2$)$_2$}] (d_3-**2**) was observed by ^1H NMR (18 h; r.t.), H/D exchange in the pincer backbone was studied by heating this sample to 80 °C and monitoring the progress of the reaction by ^1H NMR. Upon complete conversion to [Ru(D)$_2$PMe$_3$-{DN(CD$_2$CD$_2$P^{i}Pr$_2$)$_2$}] (d_{11}-**2**), D_2 was exchanged with H_2 (1 bar) to measure D/H exchange at room temperature, giving [Ru(H)$_2$PMe$_3${HN(CD$_2$CD$_2$P^{i}Pr$_2$)$_2$}] (d_8-**2**).

X-Ray Crystal Structure Determinations. Complex **1**. Crystal data and details of the structure determination: formula, $C_{19}H_{46}NP_3Ru$; M_r = 482.55; crystal color and shape, red needle; crystal dimensions = 0.08 × 0.10 × 0.51 mm; crystal system, monoclinic; space group $P2_1/c$ (no. 14); a = 14.3777(4), b = 9.9139(3), c = 17.8316(5) Å; β = 103.5144(14)°; V = 2471.32(12) Å^3; Z = 4; μ (Mo Kα) = 0.831 mm^{-1}; ρ_{calcd} = 1.297 g cm^{-3}; Θ range = 1.46−25.35; data collected, 113 859; independent data [I_o > 2σ(I_o)/all data/R_{int}], 4518/4363/0.025; data/restraints/parameters, 4518/0/401; *R*1 [I_o > 2σ(I_o)/all data], 0.0140/0.0148; *wR*2 [I_o > 2σ(I_o)/all data], 0.0348/0.0357; GOF = 1.066; $\Delta\rho_{max/min}$, 0.34/−0.33 e Å^{-3}. Complex **4**: Crystal data and details of the structure determination: formula, $C_{32}H_{74}Cl_4N_2P_4Ru_2$; M_r = 954.75; crystal color and shape, yellow prism; crystal dimensions = 0.30 × 0.51 × 0.51 mm; crystal system, monoclinic; space group $P2_1/n$ (no. 14); a = 12.4756(4), b = 13.7853(4), c = 13.0588(4) Å; β = 105.114(3)°; V = 2168.17(12) Å^3; Z = 2; μ (Mo Kα) = 1.115 mm^{-1}; ρ_{calcd} = 1.462 g cm^{-3}; Θ range = 6.04−25.35; data collected, 24 182; independent data [I_o > 2σ(I_o)/all data/R_{int}], 2219/2602/0.039; data/restraints/parameters, 2602/0/207; *R*1 [I_o > 2σ(I_o)/all data], 0.0368/0.0498; *wR*2 [I_o > 2σ(I_o)/all data], 0.0718/0.0808; GOF = 1.220; $\Delta\rho_{max/min}$, 0.61/−0.49 e Å^{-3}. Complex **5**: Crystal data and details of the structure determination: formula, $C_{19}H_{46}Cl_2NP_3Ru$; M_r = 553.45; crystal color and shape, light orange fragment; crystal dimensions = 0.23 × 0.28 × 0.38 mm; crystal system, triclinic; space group $P\bar{1}$ (no. 2); a = 9.9919(5), b = 10.4067(5), c = 13.1852(6) Å; α = 104.037(2), β = 100.273(2), γ = 101.193(2)°; V = 1267.66(11) Å^3; Z = 2; μ (Mo Kα) = 1.024 mm^{-1}; ρ_{calcd} = 1.450 g cm^{-3}; Θ range = 3.19−25.35; data collected, 66 371; independent data [I_o > 2σ(I_o)/all data/R_{int}], 4423/4478/0.047; data/restraints/parameters, 4478/0/246; *R*1 [I_o > 2σ(I_o)/all data], 0.0342/0.0344; *wR*2 [I_o > 2σ(I_o)/all data], 0.0915/0.0919; GOF = 1.250; $\Delta\rho_{max/min}$, 1.33/−0.77 e Å^{-3}. Complex **10**: Crystal data and details of the structure determination: formula, $C_{20}H_{50}NP_3Ru$; M_r = 498.59; crystal color and shape, yellow fragment; crystal dimensions = 0.33 × 0.41 × 0.43 mm; crystal system, orthorhombic; space group *Pnma* (no. 62); a = 12.7484(6), b = 19.6938(9), c = 10.1107(5) Å; V = 2538.4(2) Å^3; Z = 4; μ (Mo Kα) = 0.812 mm^{-1}; ρ_{calcd} = 1.305 g cm^{-3}; Θ range = 2.26−25.48; data collected, 70 205; independent data [I_o > 2σ(I_o)/all data/R_{int}], 2252/2376/0.031; data/restraints/parameters, 2376/0/132; *R*1 [I_o > 2σ(I_o)/all data], 0.0167/0.0183; *wR*2 [I_o > 2σ(I_o)/all data], 0.0448/0.0473; GOF = 1.126; $\Delta\rho_{max/min}$, 0.34/−0.32 e Å^{-3}. Complex **12**: Crystal data and details of the structure determination: formula, $C_{21}H_{47}F_3NO_3P_3RuS$; M_r = 644.65; crystal color and shape, yellow fragment; crystal dimensions = 0.41 × 0.46 × 0.51 mm; crystal system, monoclinic; space group $P2_1/n$ (no. 14); a = 10.2224(5), b = 19.1971(10), c = 15.5142(8) Å; β = 103.351(2)°; V = 2962.2(3) Å^3; Z = 4; μ (Mo Kα) = 0.803 mm^{-1}; ρ_{calcd} = 1.446 g cm^{-3}; Θ range = 1.72−25.32; data collected, 80 411; independent data [I_o > 2σ(I_o)/all data/R_{int}], 5218/5387/0.025; data/restraints/parameters, 5387/0/310; *R*1 [I_o > 2σ(I_o)/all data], 0.0200/0.0209; *wR*2 [I_o > 2σ(I_o)/all data], 0.0493/0.0501; GOF = 1.092; $\Delta\rho_{max/min}$, 0.45/−0.46 e Å^{-3}. CCDC 761695 (**1**), 761696 (**4**), 761697 (**5**), 761698 (**10**), and 761699 (**12**) contain the supplementary crystallographic data for this paper. These data can be obtained free of charge from The Cambridge Crystallographic Data Centre via www.ccdc.cam.ac.uk/data_request/cif.

(18) Frisch, M. J.; Trucks, G. W.; Schlegel, H. B.; Scuseria, G. E.; Robb, M. A.; Cheeseman, J. R.; Montgomery, J. A., Jr.; Vreven, T.; Kudin, K. N.; Burant, J. C.; Millam, J. M.; Iyengar, S. S.; Tomasi, J.; Barone, V.; Mennucci, B.; Cossi, M.; Scalmani, G.; Rega, N.; Petersson, G. A.; Nakatsuji, H.; Hada, M.; Ehara, M.; Toyota, K.; Fukuda, R.; Hasegawa, J.; Ishida, M.; Nakajima, T.; Honda, Y.; Kitao, O.; Nakai, H.; Klene, M.; Li, X.; Knox, J. E.; Hratchian, H. P.; Cross, J. B.; Bakken, V.; Adamo, C.; Jaramillo, J.; Gomperts, R.; Stratmann, R. E.; Yazyev, O.; Austin, A. J.; Cammi, R.; Pomelli, C.; Ochterski, J. W.; Ayala, P. Y.; Morokuma, K.; Voth, G. A.; Salvador, P.; Dannenberg, J. J.; Zakrzewski, V. G.; Dapprich, S.; Daniels, A. D.; Strain, M. C.; Farkas, O.; Malick, D. K.; Rabuck, A. D.; Raghavachari, K.; Foresman, J. B.; Ortiz, J. V.; Cui, Q.; Baboul, A. G.; Clifford, S.; Cioslowski, J.; Stefanov, B. B.; Liu, G.; Liashenko, A.; Piskorz, P.; Komaromi, I.; Martin, R. L.; Fox, D. J.; Keith, T.; Al-Laham, M. A.; Peng, C. Y.; Nanayakkara, A.; Challacombe, M.; Gill, P. M. W.; Johnson, B.; Chen, W.; Wong, M. W.; Gonzalez, C.; Pople, J. A. Gaussian, Inc.: Wallingford, CT, 2004.

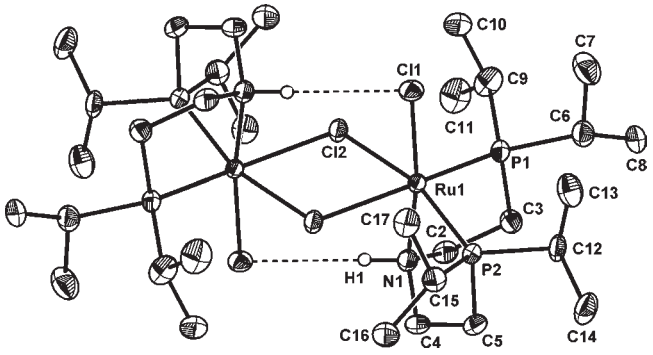

Figure 2. DIAMOND plot of **4** in the crystal with thermal ellipsoids drawn at the 50% probability level. Hydrogen atoms other than H1 are omitted for clarity.

Scheme 2. Synthesis of Complex **5**

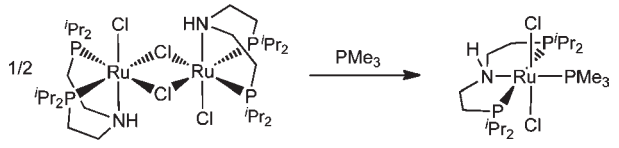

DFT Calculations. All calculations were performed with Gaussian 03, revision C.02 using the density functional/Hartree−Fock hybrid model Becke3LYP and the split valence double-ζ (DZ) basis set 6-31+G**.[18−20] The Ru atoms were described with a Stuttgart-RSC-ECP with a DZ description of the valence electrons.[21] Geometry optimizations were run without symmetry or internal coordinate constraints. The optimized structures were verified as being true minima (NImag = 0) or transition states (NImag = 1) by analysis of negative eigenvalues in vibrational frequency calculations. Thermal corrections were carried out at standard conditions (T = 298.15 K and P = 1 atm). NBO analyses were performed with NBO V3.1 as implemented in Gaussian 03.[22] Orbital expressions were visualized with GaussView via cube files generated from formatted checkpoint files.[23]

Results and Discussion

1.1. Metal−Ligand Cooperativity: Formation of PNP Enamido Complex 3. Starting from commercially available $[(Cymene)RuCl_2]_2$, precursor complex $[RuCl_2PMe_3(HPNP)]$ (**5**) is easily prepared in almost quantitative yield by ligand substitution and subsequent reaction of chloro-bridged dimer $[RuCl_2(HPNP)]_2$ (**4**) with PMe_3 (Scheme 2), as reported earlier.[10b] The molecular structures of **4** and **5** in the solid state could be derived by single-crystal X-ray diffraction (Figures 2 and 3, Table 1), confirming the structural assignments on the basis of solution NMR spectroscopy.[24] A comparison of the molecular structures

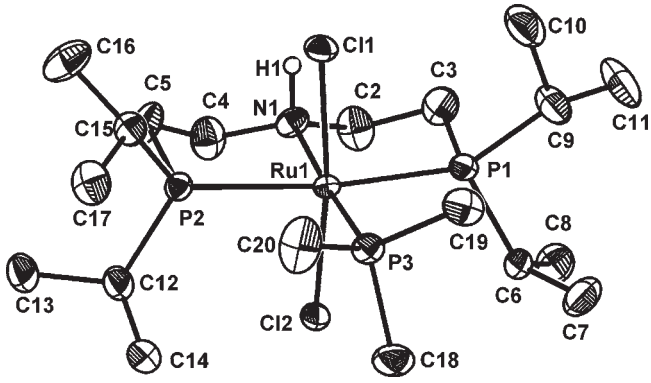

Figure 3. DIAMOND plot of **5** in the crystal with thermal ellipsoids drawn at the 50% probability level. Hydrogen atoms other than H1 are omitted for clarity.

Table 1. Selected Bond Lengths and Bond Angles of **4** and **5** in the Crystal

	4	**5**
	Bond Lengths (Å)	
Ru1−Cl1	2.442(1)	2.4312(7)
Ru1−Cl2	2.472(1)	2.4309(6)
Ru1−Cl2[a]	2.478(1)	
Ru1−N1	2.113(4)	2.186(2)
Ru1−P1	2.261(1)	2.3897(8)
Ru1−P2	2.274(1)	2.3838(8)
Ru1−P3		2.2627(8)
	Bond Angles (deg)	
N1−Ru1−P3		177.13(6)
P1−Ru1−P2	98.05(5)	163.04(3)

[a] Symmetry operation for equivalent atoms (−x, −y, −z).

demonstrates the capability of the *iso*-propyl substituted *H*PNP ligand to bind both facially and meridionally to the metal. Facial coordination as in **4** permits dimerization via chloro bridges to allow for coordinative saturation of the ruthenium(II) center. The close proximity of N1 and the terminal chloride Cl1 suggests further stabilization by N···H···Cl hydrogen bonding. The structural parameters of **4** in the crystal strongly resemble those of $[RuCl_2\{HN(CH_2CH_2PPh_2)_2\}]$.[25] The molecular structure of **5** features octahedrally coordinated ruthenium and a *trans*-dichloride configuration with small distortions mainly caused by the pincer bite angle (P1−Ru−P2 163.04(3)°), which is in the typical range for the meridonally bound *H*PNP ligand.[4f,26]

We previously reported that the reaction of **5** with KO^tBu (> 3 equiv) gives enamide **3** in quantitative yield (Scheme 3). The reaction is rapid with an immediate color change to the deep green product observed at room temperature. No intermediates are detected by ^{31}P NMR, and only incomplete conversion is obtained with smaller amounts of the base. As a likely pathway for the formation of **3**, initial dehydrohalogenation of **5** to chloroamide complex $[RuClPMe_3(PNP)]$ (**6**) is followed by β-hydride migration to give imine complex $[RuCl(H)PMe_3(PNP^*)]$

(19) (a) Vosko, S. H.; Wilk, L.; Nusair, M. *Can. J. Phys.* **1980**, *58*, 1200–1211. (b) Lee, C.; Yang, W.; Parr, R. G. *Phys. Rev. B.* **1988**, *37*, 785–789. (c) Becke, A. D. *J. Chem. Phys.* **1993**, *98*, 5648–5652.

(20) (a) Hehre, W. J.; Ditchfield, R.; Pople, J. A. *J. Chem. Phys.* **1972**, *56*, 2257–2261. (b) Francl, M. M.; Pietro, W. J.; Hehre, W. J.; Binkley, J. S.; Gordon, M. S.; DeFrees, D. J.; Pople, J. A. *J. Chem. Phys.* **1982**, *77*, 3654–3665.

(21) Dolg, M.; Stoll, H.; Preuss, H.; Pitzer, R. M. *J. Phys. Chem.* **1993**, *97*, 5852–5859.

(22) Glendening, E. D.; Reed, A. E.; Carpenter, J. E.; Weinhold, F. *NBO*, version 3.1; University of Wisconsin: Madison, WI.

(23) Dennington II, R.; Keith, T.; Millam, J. *GaussView V4.1*; Semichem Inc.: Shawnee Mission, KS, 2007.

(24) The molecular structure of **4** has recently been depicted in a patent without structural details reported: Abdur-Rashid, K.; Graham, T.; Tsang, C.-W.; Chen, X.; Guo, R.; Jia, W.; Amoroso, D.; Sui-Seng, C. WO2008/141439.

(25) Walther, D.; Klobes, O.; Stollenz, M.; Imhof, W.; Gorls, H. Private communication to the Cambridge Structural Database, **2003**.

(26) (a) Friedrich, A.; Ghosh, R.; Kolb, R.; Herdtweck, E.; Schneider, S. *Organometallics* **2009**, *28*, 708–718. (b) Meiners, J.; Friedrich, A.; Herdtweck, E.; Schneider, S. *Organometallics* **2009**, *28*, 6331–6338.

Scheme 3. Syntheses of PNP Enamido (**3**), Amido (**1**), Amine (**2**), and Imine (**7**) Complexes

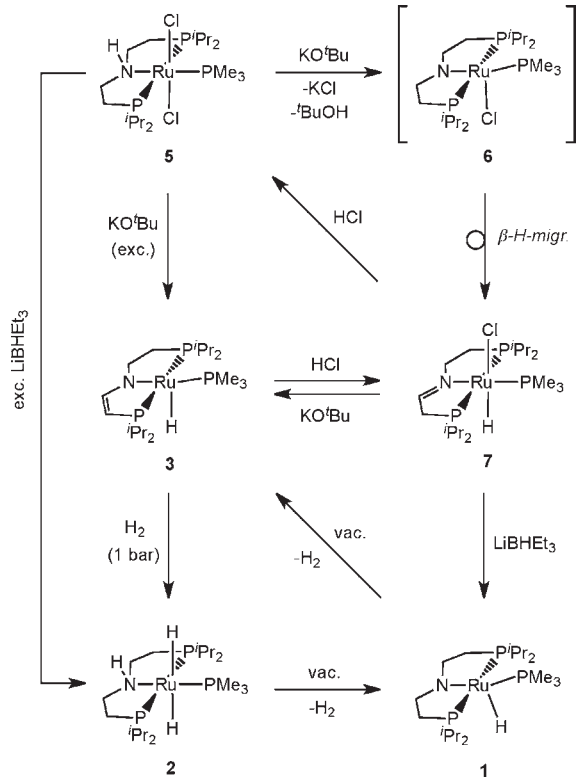

(**7**; PNP* = N(CHCH$_2$P^{i}Pr$_2$)(CH$_2$CH$_2$P^{i}Pr$_2$)). Deprotonation of **7** at the expectedly acidic γ-carbon atom (Figure 1) would then result in **3**. To check for this pathway, imine intermediate **7** was synthesized by HCl addition to **3** in isolated yields around 50%. Complex **7** is quantitatively deprotonated by KO^{t}Bu to give enamido complex **3**, supporting our proposed mechanism. Finally, reactions of **7** with 1 equiv of HCl or **3** with excess HCl give **5** selectively. ^{31}P, ^{1}H, and ^{13}C NMR spectra of **7** confirm the C_1 symmetry and meridional arrangement of the PNP* pincer ligand. The two chelate ^{31}P NMR signals exhibit a typical *trans* $^2J_{PP}$ coupling constant (281 Hz), and the mutual *trans*-configuration of the hydrido and the chloro ligands was confirmed by ^{1}H NOESY NMR. This structural assignment of **7** is further supported by X-ray diffraction. However, the crystal was disordered with respect to the position of the N=C double bond in the pincer backbone, preventing a detailed structural discussion (Supporting Information).

Milstein and co-workers have shown that PNP pincer complexes of the type [RuH(CO)Cl{NC$_5$H$_3$-2-CH$_2$PR$_2$-6-CH$_2$ER′$_2$}] (R = ^{i}Pr, ^{t}Bu; ER′$_2$ = NEt$_2$, P^{i}Pr$_2$) can be deprotonated at the pincer backbone in the benzylic position to give [RuH(CO){NC$_5$H$_3$-2-CHPR$_2$-6-CH$_2$ER′$_2$}],[27] which is a highly active catalyst for carbonyl group hydrogenation, acceptor-less alcohol dehydrocoupling, and water oxidation.[27,28] For these reactions, mechanisms have been proposed, where reversible proton transfer at the pincer backbone is a decisive step in the catalytic cycles. Furthermore, ligand cooperativity was demonstrated for both H_2 and benzene addition to [Ir(COE)-{NC$_5$H$_3$-2-CH$_2$P^{i}Pr$_2$-6-CHP^{i}Pr$_2$}], where proton shifts to the deprotonated benzylic position of the pincer ligand were observed upon H−H and C−H bond activation.[29] Benzylic deprotonation of such pyridine based PNP pincer complexes was further reported for nickel, platinum, and copper complexes.[30] Similarly, the facile double deprotonation of iridium bis(picolyl)amine complex [Ir{HN-(CH$_2$Py)$_2$}(cod)]$^+$ (cod = cyclooctadiene) in the benzylic position to give [Ir{N(CHPy)(CH$_2$Py)(cod)]$^-$ is stabilized by delocalization of the negative charge with the pyridyl substituent.[31] In this context, complex **3** represents an aliphatic analogue, suggesting that the aromaticity as in pyridine based pincer ligands does not define a general prerequisite for such proton shift reactions.

1.2. Metal−Ligand Cooperativity: Reversible Double H_2 Elimination/Addition. As a major difference with Milstein's pyridine based system, **1**, **2**, and **3** formally exhibit two functional groups in the pincer backbone (the amine group and the ethylene bridge), which are capable of promoting bifunctional heterolytic hydrogen activation, allowing for the reversible addition of 2 equiv of H_2 to **3** (Scheme 1). For the conversion of **3** to **1**, dihydrido imine complex [Ru(H)$_2$PMe$_3$(PNP*)] (**8**) seems to be a likely intermediate after proton transfer from H_2 initially binding at the free coordination site of **3** to the γ-carbon atom (Scheme 4). However, we could not find spectroscopic evidence for this compound. Furthermore, the reaction of **7** with Li[BHEt$_3$] gives amido complex **1** in high yield (Scheme 3), suggesting that **8** might be unstable with respect to the formation of amido isomer **1**.

The hydrogen elimination/addition equilibra (Scheme 1) were examined by H/D exchange experiments. Selectively deuterated [Ru(D)$_2$PMe$_3$(DN(CH$_2$CH$_2$P^{i}Pr$_2$)$_2$)] (d_3-**2**) can be prepared by the reaction of **1** with D_2 at room temperature. Under these reaction conditions, no incorporation of deuterium into the pincer backbone is observed within 18 h. Upon heating of d_3-**2** to 80 °C under D_2, slow H/D exchange of the PNP pincer backbone protons vs deuterium is observed with slightly different rates for the NCH$_2$ (k = 0.51 h^{-1}; 80 °C) and PCH$_2$ (k = 0.03 h^{-1}; 80 °C) groups, respectively (Scheme 5 and Figure 4). Finally, exposure of the fully backbone deuterated isotopomer [Ru(D)$_2$PMe$_3$(DN(CD$_2$CD$_2$P^{i}Pr$_2$)$_2$)] (d_{11}-**2**) to H_2 at room temperature results in rapid D/H exchange of the Ru−D and N−D protons ($t_{1/2}$ < 5 min; r.t.), giving [Ru(H)$_2$PMe$_3$(HN(CD$_2$CD$_2$P^{i}Pr$_2$)$_2$)] (d_8-**2**). Interstingly,

(27) (a) Zhang, J.; Leitus, G.; Ben-David, Y.; Milstein, D. *J. Am. Chem. Soc.* **2005**, *127*, 10840–10841. (b) Zhang, J.; Leitus, G.; Ben-David, Y.; Milstein, D. *Angew. Chem.* **2006**, *118*, 1131–1133. Zhang, J.; Leitus, G.; Ben-David, Y.; Milstein, D. *Angew. Chem., Int. Ed.* **2006**, *45*, 1113−1115.

(28) (a) Gunanathan, C.; Ben-David, Y.; Milstein, D. *Science* **2007**, *317*, 790–792. (b) Kohl, S. W.; Weiner, L.; Schwartsburd, L.; Konstantinovski, L.; Shimon, L. J. W.; Ben-David, Y.; Iron, M. A.; Milstein, D. *Science* **2009**, *324*, 74–77.

(29) (a) Ben-Ari, E.; Leitus, G.; Shimon, L. J. W.; Milstein, D. *J. Am. Chem. Soc.* **2006**, *128*, 15390–15391. (b) Iron, M. A.; Ben-Ari, E.; Cohen, R.; Milstein, D. *Dalton Trans.* **2009**, 9433–9439. (c) Zeng, G.; Guo, Y; Li, S *Inorg. Chem.* **2009**, *48*, 10257–10263.

(30) (a) Vuzman, D.; Poverenov, E.; Shimon, L. J. W.; Diskin-Posner, Y.; Milstein, D. *Organometallics* **2008**, *27*, 2627–2634. (b) van der Vlugt, J. I.; Lutz, M.; Pidko, E. A.; Vogt, D.; Spek, A. L. *Dalton Trans.* **2009**, 1016–1023. (c) van der Vlugt, J. I.; Pidko, E. A.; Vogt, D.; Lutz, M.; Spek, A. L. *Inorg. Chem.* **2009**, *48*, 7513–7515.

(31) (a) Tejel, C.; Ciriano, M. A.; del Río, M. P.; Hetterscheid, D. G. H.; Tsichlis i Spithas, N.; Smits, J. M. M.; de Bruin, B. *Chem.—Eur. J.* **2008**, *14*, 10932–10936. (b) Tejel, C.; del Río, M. P.; Ciriano, M. A.; Reijerse, E. J.; Hartl, F.; Záliš, S.; Hetterscheid, D. G. H.; Tsichlis i Spithas, N.; de Bruin, B. *Chem.—Eur. J.* **2009**, *15*, 11878–11889.

Scheme 4. Possible Intermediate **8** for Hydrogenation of **3** to **1**

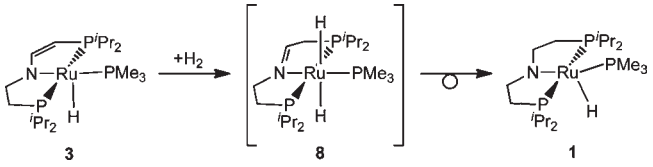

Scheme 5. H/D Exchange Experiments

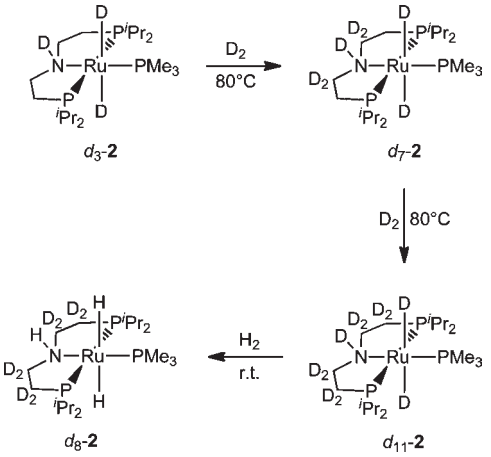

both hydride ligands exhibit the same rates of exchange, which cannot be simply explained by reversible Ru−H/N−H syn H_2 elimination/addition. Therefore, a 2D ^{1}H NOESY spectrum of **2** in d_8-THF under H_2 (1 bar) was obtained (Supporting Information). The spectrum features exchange cross peaks of the two hydride ligands with each other and of the hydride, which is adjacent to the PNP N−H proton, with H_2. This result is in agreement with Ru−H/N−H syn H_2 elimination/addition and scrambling of the two hydride ligands, e.g., via amine inversion.[32] On the contrary, Ru−H/H_2 exchange upon phosphine dissociation should not be stereoselective and give exchange cross peaks of H_2 with *both* hydride ligands.

Precise evaluation of the H/D exchange kinetic data is hampered by superimposition of pincer backbone ^{1}H signals with other peaks (Figure 4). However, comparison of the relative rates for Ru−H and N−H vs pincer backbone C−H H/D exchange provides valuable information: H/D exchange for the pincer backbone protons exhibits sizable activation energies, with a slightly higher barrier for the PCH_2 as compared to the NCH_2 group. Most importantly, no stereoselectivity for the diastereotopic NCH_2 and PCH_2 protons of **2** is found, indicating that the exchange proceeds via a C_{2v} symmetric intermediate, such as imine complex **8**.[33] Furthermore, these barriers are considerably higher as compared with exchange of the Ru−H and N−H moieties.

To gain further insight into the interconversion of **1**, **2**, and **3** and the possible involvement of **8**, DFT calculations (B3LYP/6-31+G**) on a somewhat simpler model

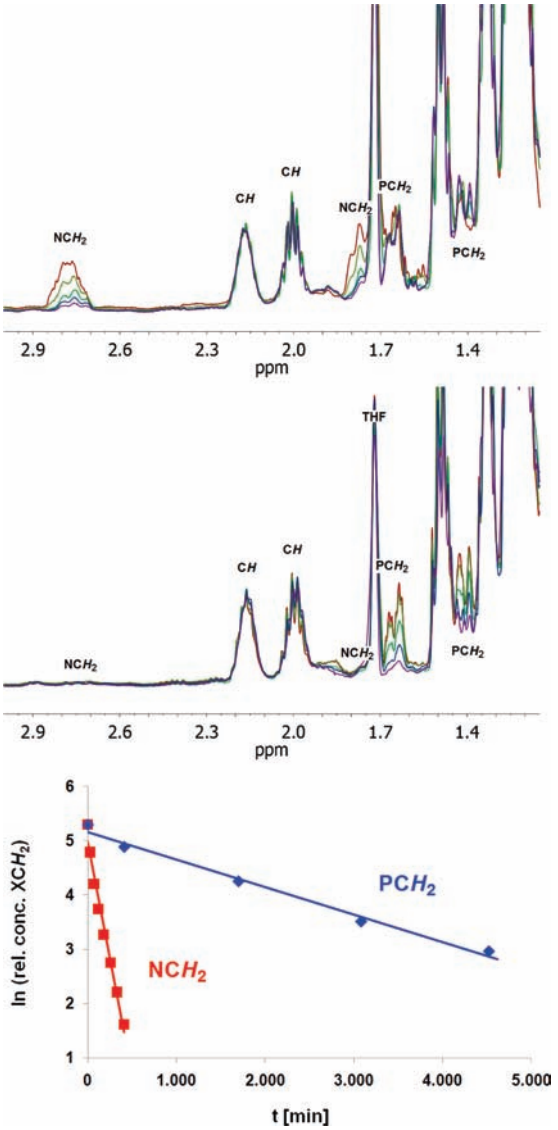

Figure 4. Top: Progress of NCH_2 H/D exchange of d_3-**2** monitored by ^{1}H NMR in d_8-THF (1 bar D_2, 80 °C) after 0 min (red), 30 min (light green), 70 min (green), 120 min (blue), and 180 min (purple). Center: Progress of PCH_2 H/D exchange of d_7-**2** monitored by ^{1}H NMR in d_8-THF (1 bar D_2, 80 °C) after 410 min (red), 660 min (light green), 1700 min (green), 3080 min (blue), and 4520 min (purple). Bottom: First order kinetic plots for NCH_2 (2.8 ppm) and PCH_2 (1.65 ppm) ^{1}H NMR peak integrals.

with PMe_2 instead of P^iPr_2 substituents on the pincer ligand were carried out. The barriers for the elementary steps of the sequence $\mathbf{2^{Me} \leftrightarrow TS(2^{Me}/1^{Me}\text{-}H_2) \leftrightarrow 1^{Me}\text{-}H_2 \leftrightarrow TS(1^{Me}\text{-}H_2/1^{Me}) \leftrightarrow 1^{Me} \leftrightarrow TS(1^{Me}/8^{Me}) \leftrightarrow 8^{Me} \leftrightarrow TS(8^{Me}/3^{Me}\text{-}H_2) \leftrightarrow 3^{Me}\text{-}H_2 \leftrightarrow TS(3^{Me}\text{-}H_2/3^{Me}) \leftrightarrow 3^{Me}}$ are displayed in Scheme 6. Gusev and co-workers recently examined hydrogen shift reactions in the backbone of related PCP ruthenium pincer complexes.[34] The proposed mechanism was composed of a sequence of α- and β-H migration reactions, interconverting ruthenium(II) olefin hydrido, carbene hydrido, and alkyl isomers. Most interestingly, the authors showed that the four-coordinate 14-electron alkyl intermediates exhibit an energetically low lying triplet ground state resulting in very low barriers

(32) In the presence of water, we proposed for O−H/N−H proton exchange of **2** to account for amine inversion. However, sharp ^{1}H NMR signals for the Ru−H protons during reaction monitoring suggest the absence of water in the sample (reference 7c).

(33) Owing to the considerably different rates for Ru−H, NCH_2, and PCH_2 H/D exchange, respectively, seconadary isotope effects can be neglected.

(34) Kuznetsov, V. F.; Abdur-Rashid, K.; Lough, A. J.; Gusev, D. G. *J. Am. Chem. Soc.* **2006**, *128*, 14388–14396.

Scheme 6. DFT Results for the Mechanism of H_2 Elimination (2 equiv) from $\mathbf{2^{Me}}$ in the Gas Phase (Energies for PCM Solvent Correction in Parentheses)

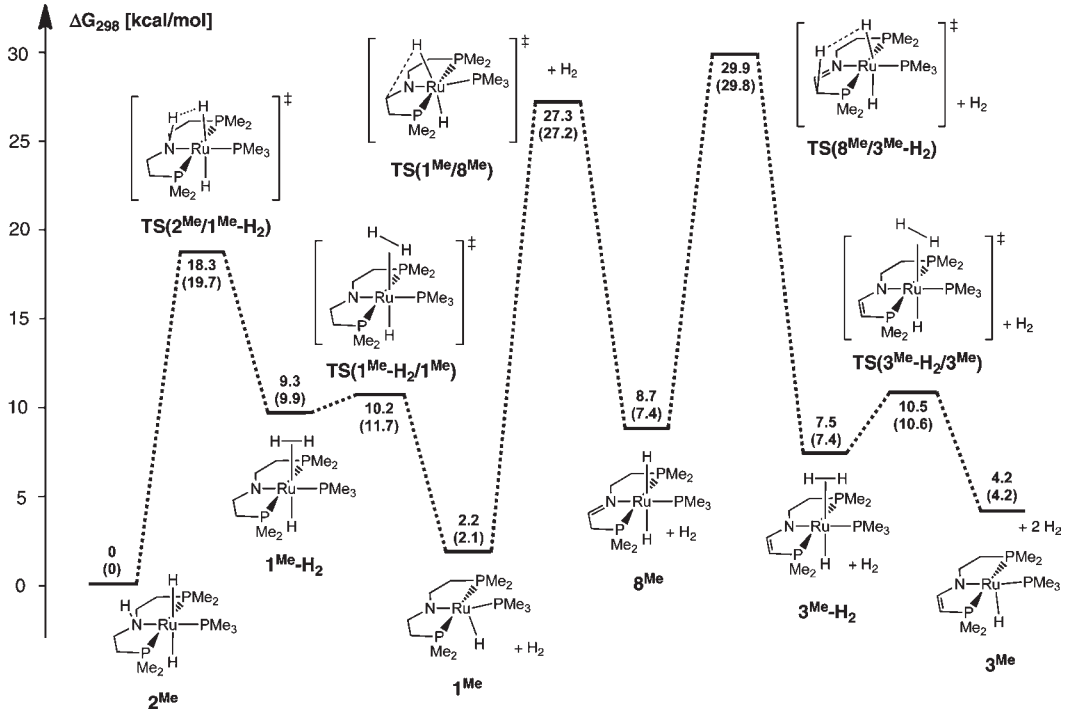

of isomerization.[35] However, in contrast to that system, in the present case, all intermediates are formally 18- or 16-electron complexes, respectively. Accordingly, single-point calculations for all ground state geometries in the triplet state resulted in higher energies by 44−74 kcal/mol (Supporting Information).[36] Therefore, it is reasonable to assume for all reactions to be located on a singlet potential energy surface (PES).

Overall, elimination of 2 equiv of H_2 from $\mathbf{2^{Me}}$ via $\mathbf{1^{Me}}$ to $\mathbf{3^{Me}}$ was calculated to be almost thermoneutral with $\Delta G_{\mathbf{2\rightarrow 1}} = +2.2$ and $\Delta G_{\mathbf{1\rightarrow 3}} = +2.0$ kcal/mol, respectively. Hydrogen elimination from amine $\mathbf{2^{Me}}$ to amide $\mathbf{1^{Me}}$ proceeds via proton transfer from the N−H moiety to a ruthenium bound hydride with a moderate barrier (18.3 kcal/mol) followed by an almost barrierless H_2 loss of dihydrogen complex $\mathbf{1^{Me}}$**-H$_2$** (0.9 kcal/mol).[10b] This result is in qualitative agreement with the H/D exchange experiments at room temperature. For the $\mathbf{1^{Me} \Leftrightarrow 3^{Me}}$ branch of the H_2-elimination sequence, dihydrido imine complex [Ru(H)$_2$PMe$_3$(PNP*)] ($\mathbf{8^{Me}}$) was found to be a minimum on the PES but unstable with respect to both a loss of dihydrogen toward enamide **3** ($\Delta G_{\mathbf{8\rightarrow 3}} = -4.5$ kcal/mol) and isomerization to amide **1** ($\Delta G_{\mathbf{8\rightarrow 1}} = -6.5$ kcal/mol). Hence, thermodynamics explain why **8** cannot not be detected as an intermediate experimentally. The sizable calculated barriers for **TS**($\mathbf{8^{Me}/3^{Me}}$**-H$_2$**) and **TS**($\mathbf{1^{Me}/8^{Me}}$) are in agreement with the slow H/D exchange found for the pincer backbone protons. Furthermore, the higher calculated barrier for **TS**($\mathbf{8^{Me}/3^{Me}}$**-H$_2$**) over **TS**($\mathbf{1^{Me}/8^{Me}}$) ($\Delta\Delta G^{\ddagger} = 2.6$ kcal/mol) provides an explanation for the higher experimental rate of NCH_2 over PCH_2 H/D exchange, since both hydride ligands of **2** undergo H/D exchange with higher rates than backbone C−H activation. As for H_2-elimination from amido dihydrogen complex $\mathbf{1^{Me}}$**-H$_2$**, elimination from enamido dihydrogen intermediate $\mathbf{3^{Me}}$**-H$_2$** proceeds with a very small barrier ($\Delta G^{\ddagger}_{\mathbf{TS3\text{-}H2/3}} = 3.0$ kcal/mol) to complete the sequence $\mathbf{2^{Me} \Leftrightarrow 1^{Me}}$**-H$_2$** $\Leftrightarrow \mathbf{1^{Me}} + H_2 \Leftrightarrow \mathbf{8^{Me}} + H_2 \Leftrightarrow \mathbf{3^{Me}}$**-H$_2$** $+ H_2 \Leftrightarrow \mathbf{3^{Me}} + 2\ H_2$. Our theoretical results demonstrate that the pincer ligand N−H and C−H activation processes via proton shifts to hydride ligands and β-hydrogen migration are thermally accessible even without predissociation of one of the pincer ligand "arms".

We have shown previously that Brønsted acids, such as water, can catalyze the formation of dihydrogen complex $\mathbf{1^{Me}}$**-H$_2$** by hydrogen bonding with the amine and the hydride ligands.[7c] Likewise, Iron, Milstein, and co-workers recently reported theoretical results suggesting that water considerably lowers the barrier of oxidative proton transfer from a benzylic methylene group to the metal in a pyridine based PNP−iridium complex.[29b] Therefore, acceleration of the right branch of the $\mathbf{2^{Me} \Leftrightarrow 1^{Me} \Leftrightarrow 3^{Me}}$ sequence by trace amounts of Brønsted acids, such as water, cannot be fully excluded. However, from the slow H_2 loss from **1** at room temperature reported earlier,[10b] a first order half-life of approx $t_{1/2} \approx 9$ d ($k \approx 0.0036\ h^{-1}$) can be estimated. Hence, the corresponding barrier ($\Delta G^{\ddagger} \approx$ 28 kcal/mol) is in good agreement with the calculated barriers for the model **TS**($\mathbf{1^{Me}/8^{Me}}$) and **TS**($\mathbf{8^{Me}/3^{Me}}$**-H$_2$**). Furthermore, the sharp ^{1}H NMR peaks observed for the hydride ligands during H/D exchange experiments indicate the absence of water.[7c] Therefore, Brønsted acid catalysis was not examined theoretically for this step.

In contrast to dihydrido imine complex **8**, hydrido chloro imine **7** could be isolated and fully characterized. The preference for imine isomer **7** is attributed to the

(35) A rare example of a square-planar ruthenium(II) complex with a triplet ground state: Watson, L. A.; Ozerov, O. V.; Pink, M.; Caulton, K. G. *J. Am. Chem. Soc.* **2003**, *125*, 8426–8427.

(36) Even for four-coordinate, square-planar complex [RuCl{N(CH$_2$CH$_2$-P^{t}Bu$_2$)$_2$}] a singlet ground state was found experimentally: Askevold, B.; Khusniyarov, M. M.; Herdtweck, E.; Meyer, K.; Schneider, S. Submitted.

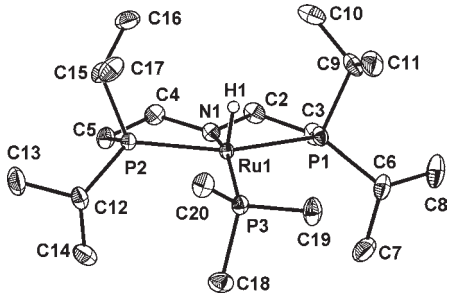

Figure 5. DIAMOND plot of **1** in the crystal with thermal ellipsoids drawn at the 50% probability level. Hydrogen atoms other than H1 are omitted for clarity.

reduced hydridicity of the hydride ligand owing to the smaller *trans* influence of the chloride ligand as compared to dihydride **8**. Ground-state destabilization of the imine hydride by a strong *trans*-ligand to the hydride might therefore be an important structural feature for Noyori-type hydrogenation catalysts to prevent rapid catalyst deactivation by imine formation.[13]

2.1. Enamido (3) vs Amido (1) Complex: Comparison of the Structures. The facile synthesis of enamide **3** is particularly interesting since enamido ligand PNP' was unknown prior to this template synthesis.[37] Therefore, a comparison of the molecular and electronic structures could provide valuable information to rationalize the reactivities (*vide infra*) of the related PNP amido and enamido complexes.

Despite the high relevance of five-coordinate 16-electron ruthenium(II) hydrido amido complexes like **1** in hydrogenation reactions with Noyori−Morris-type catalysts,[6] only very few examples have been structurally characterized by X-ray diffraction.[7a,38] Suitable single crystals of **1** were grown by slow cooling of a pentane solution to −40 °C (Figure 5 and Table 2). The high quality of the diffraction data allowed for independent location and refinement of the hydride ligand. The coordination polyhedron around the metal can best be described as a Y-shaped distorted trigonal-bipyramid (Y-TBP) with N1, H1, and P3 defining the equatorial ligands and with distortion from the ideal TBP arising from the small H1−Ru−P3 angle (76.0(7)°) and large H1−Ru−N1 (124.8(7)°) and N1−Ru−P3 (159.12(3)°) angles. Such Y-TBP coordination polehedra are typically found for diamagnetic five-coordinate

Table 2. Selected Bond Lengths and Bond Angles of **1** in the Crystal and in the DFT Models (B3LYP/6-31+G**) of **1** and **3**

	1	$\mathbf{1}^{DFT}$	$\mathbf{3}^{DFT}$
	Bond Lengths (Å)		
Ru1−H	1.49(2)	1.59	1.59
Ru1−N1	2.023(1)	2.07	2.13
Ru1−P1	2.3077(3)	2.36	2.37
Ru1−P2	2.2996(4)	2.36	2.43
Ru1−P3	2.2629(4)	2.34	2.32
	Bond Angles (Å)		
H1−Ru1−P3	76.0(7)	79.7	84.6
H1−Ru1−N1	124.8(7)	119.1	102.5
N1−Ru1−P3	159.12(3)	161.1	172.6
P1−Ru1−P2	160.57(1)	160.5	159.0

d^6 complexes with one strongly π-donating ligand in *trans*-position to the smallest bond angle, such as in [IrCl(H)-Me(PCy_3)$_2$] or [Ir(^{i}Pr)$_2${N($SiMe_2CH_2PPh_2$)$_2$}].[39] The Y-TBP conformation is preferred over T-shaped distortion owing to stabilization of the amide nitrogen lone pair p orbital by interaction with the empty metal d_{xy} orbital (Figure 6).[40] However, some deformation of the Y-TBP toward a T-shaped (*viz*., square pyramidal, SP) geometry in **1** most likely arises from steric interactions of the PMe_3 ligand with the pincer ^{i}Pr substituents, as suggested by a space filling model. Similarly, the Ru−N1 distance (2.023(1) Å) points toward increased steric crowding, as compared with [RuH($HNCMe_2CMe_2NH_2$)(PPh_3)$_2$] (Ru−N_{amide} = 1.967(1) Å),[7a] but is considerably shorter compared with amine complex **5** (Ru−N1 = 2.186(2) Å).

Since enamide **3** could not be crystallized to date, full models of **1** and **3** were calculated by DFT methods (B3LYP/6-31+G**). The structure of **1** agrees reasonably well with the experimental data from X-ray diffraction (Table 2).[41] Furthermore, the structural parameters around the metal centers of the optimized geometries of **1** and **3** are only marginally different compared with the simpler, PMe_2-substituted models used in section 2.1. Analysis of the frontier orbitals confirms the simple qualitative picture described above (Supporting Information). The HOMO of **1** is mostly represented by the metal $d_{x^2-y^2}$ orbital, while the LUMO is composed of contributions by the metal d_{xy} orbital and the nitrogen *p* orbital, further increasing the HOMO−LUMO gap.

In contrast to **1**, **3** exhibits a structure much closer to SP coordination of the metal with the hydride ligand in the apical position, as documented by the H1−Ru−N1 ($\mathbf{1}^{DFT}$, 119.1°; $\mathbf{3}^{DFT}$, 102.5°) and N1−Ru−P3 angles

(37) Monoanionic PN enamido ligands with an aliphatic chelate backbone have been reported: (a) Braunstein, P.; Pietsch, J.; Chauvin, Y.; Mercer, S.; Saussine, L.; DeCian, A.; Fischer, J. *J. Chem. Soc., Dalton Trans.* **1996**, 3571–3574. (b) Coleman, K. S.; Green, M. L. H.; Pascu, S. I.; Rees, N. H.; Cowley, A. R.; Rees, L. H. *J. Chem. Soc., Dalton Trans.* **2001**, 3384–3395. (c) Pascu, S. I.; Anderson, G. D. W.; Green, M. L. H.; Green, J. C.; Rees, N. H.; Cowley, A. R. *Inorg. Chim. Acta* **2006**, *359*, 3677–3692. (d) Wang, Z.-X.; Wang, L. *Chem. Commun.* **2007**, 2423–2425.

(38) (a) Haack, K.-J.; Hashiguchi, S.; Fujii, A.; Ikariya, T.; Noyori, R. *Angew. Chem.* **1997**, *109*, 297–300. *Angew. Chem., Int. Ed. Engl.* **1997**, *36*, 285-288. (b) Fryzuk, M. D.; Petrella, M. J.; Coffin, R. C.; Patrick, B. O. *C. R. Chim.* **2002**, *5*, 451–460. (c) Watson, L. A.; Coalter, J. N., III; Ozerov, O.; Pink, M.; Huffman, J. C.; Caulton, K. G. *New J. Chem.* **2003**, *27*, 263–273. (d) Li, T.; Churlaud, R.; Lough, A. J.; Abdur-Rashid, K.; Morris, R. H. *Organometallics* **2004**, *23*, 6239–6247. (e) Çelenligil-Çetin, R.; Watson, L. A.; Guo, C.; Foxman, B. M.; Ozerov, O. V. *Organometallics* **2005**, *24*, 186–189. (f) Boubekeur, L.; Ulmer, S.; Ricard, L.; Mézailles, N.; Le Floch, P. *Organometallics* **2006**, *25*, 315–317. (g) Zhang, G.; Leitus, J.; Ben-David, Y.; Milstein, D. *Angew. Chem.* **2006**, *118*, 1131–1133. Zhang, J.; Leitus, G.; Ben-David, Y.; Milstein, D. *Angew. Chem., Int. Ed.* **2006**, *45*, 1113−1115. (h) Hadzovic, A.; Song, D.; MacLaughlin, C. M.; Morris, R. H. *Organometallics* **2007**, *26*, 5987–5999.

(39) (a) Werner, H.; Höhn, A.; Dziallas, M. *Angew. Chem.* **1986**, *98*, 1112–1114. Werner, H.; Höhn, A.; Dziallas, M. *Angew. Chem., Int. Ed. Engl.* **1986**, *25*, 1090−1092. (b) Fryzuk, M. D.; McNeil, P. A.; Ball, R. G. *J. Am. Chem. Soc.* **1986**, *108*, 6414–6416.

(40) (a) Thorn, D. L.; Hoffmann, R. *New J. Chem.* **1979**, *3*, 39–45. (b) Riehl, J. F.; Jean, Y.; Eisenstein, O.; Pélessier, M. *Organometallics* **1992**, *11*, 729–737. (c) Jean, Y. In *Molecular Orbitals of Transition Metal Complexes*; Oxford University Press: Oxford, U. K., 2005.

(41) In a preliminary communication, we had reported DFT models of **1** and **3** at the B3LYP/6-31+G** level of theory (ref 10b). There, the optimized geometry of **1** adopted a slightly different conformation of the chelate ethylene bridges as compared with the experimentally derived molecular structure. However, the bond lengths and angles around the metal are in good agreement with the calculated structure presented here, which reflects the same conformation as the structural model from X-ray diffraction and represents the global minimum.

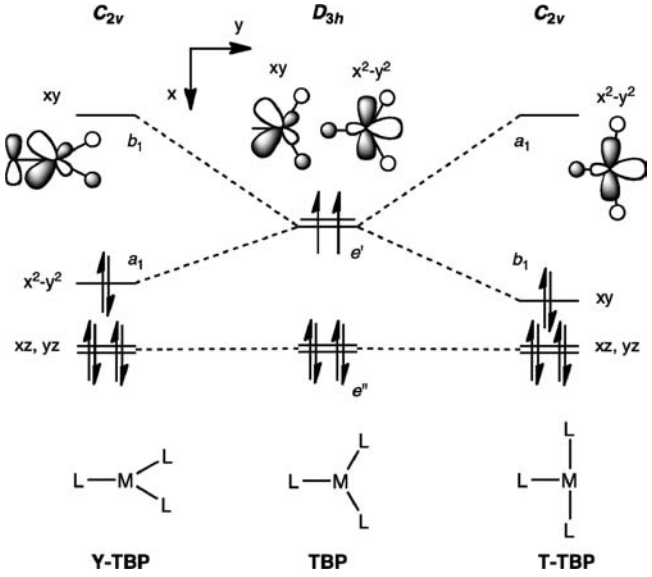

Figure 6. Qualitative Walsh diagram illustrating the splitting of the degenerate e′ orbitals in trigonal-bipyramidal (TBP) geometry upon Y-shaped and T-shaped distortion, respectively. Interaction of the LUMO in the Y-TBP case with a single-faced π-donor is indicated. Axial ligands of the TBP are omitted for clarity. Please note that the orbital denotations refer to the coordinate system of the TBP structure (D_{3h}).

($\mathbf{1}^{\mathbf{DFT}}$, 161.1°; $\mathbf{3}^{\mathbf{DFT}}$, 172.6°), respectively. Accordingly, the frontier orbital diagram shows the typical features of the T-TBP geometry with a low-lying LUMO, having a high $d_{x^2-y^2}$ contribution (Supporting Information). The smaller HOMO−LUMO gap of **3** is further expressed in the different colors of red **1** and green **3**, respectively. The notably different structures of strongly related complexes **1** and **3** can be rationalized in terms of π-donation by the PNP chelate: While the electronic and molecular structures of **1** point toward strong N→M π-donation, in the case of **3** they suggest highly reduced N→M π-donation, owing to delocalization of the *N*-lone pair by conjugation with the C=C double bond in the enamido ligand. Accordingly, the HOMO of **3** exhibits a strong contribution of a C=C γ-carbon atom p orbital. Furthermore, the Wiberg bond indices (WBI's) of the Ru−N bonds (**1**, 0.50; **3**, 0.37) and of the ligand backbone N−C (**1**, 1.02; **3**, 1.31) and C−C (**1**, 1.02; **3**, 1.60) bonds of **1** as compared with the dehydrogenated branch of **3** support reduced amide to metal π-bonding and N−C−C π-delocalization in **3**. In this context, enamido ligand PNP′ can be considered as a transition between the strongly π-donating alkylamido ligand PNP and the acceptor *N*-substituted, moderately π-donating amido pincer ligands, such as silylamides $N(SiMe_2CH_2PR_2)_2$ or arylamides $N(C_6H_4\text{-}2\text{-}PR_2)_2$.[42,43]

2.2. Enamido (3) vs Amido (1) Complex: Comparison of Reactivities. The tunable π-donating ability of the PNP ligands, which is displayed in the electronic and molecular structures, should also be expressed in the chemical reactivity of **1** and **3**. Therefore, their reactivities with electrophiles and nucleophiles were examined exemplarily by reactions with MeOTf and PMe_3, respectively.

Owing to the high electron density at the nitrogen atom, pronounced *N*-centered nucleophilicity can be expected for amido complexes of transition metals with high d-electron counts. Accordingly, stoichiometric C−N coupling of d^8 amides with carbon electrophiles is well established.[4a,f] Furthermore, in Hartwig−Buchwald-type C−N cross-coupling, amine reductive elimination by nucleophilic attack of an amido ligand at the aryl electrophile defines the selectivity determining step.[44] In a preliminary communication, we recently reported the synthesis of ruthenium(II) dihydride [Ru(H)$_2$PMe$_3$(*Me*PNP)] (**10**; *Me*PNP = MeN(CH$_2$CH$_2$P^{i}Pr$_2$)$_2$) starting from **1** by *N*-methylation with MeOTf and subsequent salt metathesis with NaH (Scheme 7).[7c] The molecular structure of **10** in the solid state (Figure 7 and Table 3) confirms the structural assignments of **10** in solution, viz., the meridional arrangement of the *Me*PNP chelate ligand and the *trans*-dihydride configuration. The longer Ru−N1 distance (2.270(2) Å) in **10**, as compared with **5** (Ru−N1, 2.186(2) Å) is compensated by shorter Ru−P_{PNP} bonds (**10**, 2.3011(4) Å; **5**, 2.3897(8) and 2.3838(8) Å), possibly reflecting increased backbonding to the phosphines in the more electron-rich dihydride.

The *N*-centered reactivity of **1** with electrophiles reflects the shape of the HOMO and the NPA charge of the nitrogen atom (−0.67*e*). However, for enamide **3**, two centers, i.e., the nitrogen atom (NPA charge: −0.65*e*) and the γ-carbon atom (NPA charge: −0.81*e*), exhibit considerable contributions to the HOMO (Supporting Information). Hence, electrophiles could attack at either of the two sites. In analogy to the backbone-saturated complex [RuH(OTf)PMe$_3$(*Me*PNP)] (**11**), complex [RuH(OTf)PMe$_3$(*Me*PNP′)] (**12**; *Me*PNP′ = MeN(CHCHP^{i}Pr$_2$)(CH$_2$CH$_2$P^{i}Pr$_2$)) is obtained from the reaction of **3** with MeOTf upon *N*-methylation in isolated yields around 40% (Scheme 8). Monitoring the reaction by ^{31}P NMR reveals that, besides **12** (∼70%), two major side products are formed, accounting for around 20% (**13a**) and 5% (**13b**) of the yield, respectively (Figure 8). Like enamine complex **12**, both side products exhibit an asymmetric PNP ligand with typical $^2J_{PP}$ *trans* coupling constants of 262 Hz (**13a**) and 261 Hz (**13b**), respectively.[45] Furthermore, both exhibit one hydride signal and a signal assignable to a N=C−H imine proton. While **13a** and **13b** could not be isolated, the spectroscopic data are in agreement with an assignment to the two diastereomeric imine complexes, resulting from nucleophilic attack of MeOTf at the enamido γ-carbon atom. Interestingly, van der Vlugt et al. recently reported that the reaction of pyridine based PNP pincer complex [Cu{C$_5$H$_3$N(2-CH$_2$P^{t}Bu$_2$)(5-CHP^{t}Bu$_2$)}] (**A**) with MeOTf

(42) (a) Liang, L.-C. *Coord. Chem. Rev.* **2006**, *250*, 1152–1177. (b) Whited, M. T.; Grubbs, R. H. *Acc. Chem. Res.* **2009**, *42*, 1607–1616.

(43) For further references, c.f. 4f and 26a.

(44) (a) Hartwig, J. F. *Acc. Chem. Res.* **1998**, *31*, 852–860. (b) Hartwig, J. F. *Synlett* **2006**, 1283–1294. (c) Corbet, J.-P.; Mignani, G. *Chem. Rev.* **2006**, *106*, 2651–2710. (d) Hartwig, J. F. *Inorg. Chem.* **2007**, *46*, 1936–1947.

(45) Selected spectroscopic data of **13a**: NMR (C_6D_6, r.t., [ppm]). ^{1}H NMR (399.8 MHz): δ −24.76 (q, $^2J_{HP}$ = 23.2 Hz, 1H, RuH), 3.16 (s, 3H, CHC*H*$_3$), 7.40 (dd, $^3J_{HP}$ = 23.5 Hz, $^4J_{HP}$ = 5.9 Hz, 1H, N=C*H*). ^{31}P {^{1}H} NMR (161.83 MHz): δ 78.0 (dd, $^2J_{PP}$ = 262.4 Hz, $^2J_{PP}$ = 28.8 Hz, CHP^{i}Pr$_2$), 71.1 (dd, $^2J_{PP}$ = 262.4 Hz, $^2J_{PP}$ = 28.8 Hz, CH$_2$P^{i}Pr$_2$), 8.5 (t, $^2J_{PP}$ = 28.8 Hz, *P*(CH$_3$)$_3$). Spectroscopic data of **13b**: NMR (C_6D_6, r.t., [ppm]). ^{1}H NMR (399.8 MHz): δ −24.76 (q, $^2J_{HP}$ = 23.2 Hz, 1H, RuH), 3.21 (s, 3H, CHC*H*$_3$), 7.62 (dd, $^3J_{HP}$ = 21.1 Hz, $^4J_{HP}$ = 5.6 Hz, 1H, N=C*H*). ^{31}P {^{1}H} NMR (161.83 MHz): δ 72.5 (dd, $^2J_{PP}$ = 260.6 Hz, $^2J_{PP}$ = 29.0 Hz, P^{i}Pr$_2$), 69.3 (dd, $^2J_{PP}$ = 260.6 Hz, $^2J_{PP}$ = 29.0 Hz, P^{i}Pr$_2$), 9.3 (t, $^2J_{PP}$ = 29.0 Hz, *P*(CH$_3$)$_3$).

Scheme 7. Synthesis of Amine Complex **10**[7c]

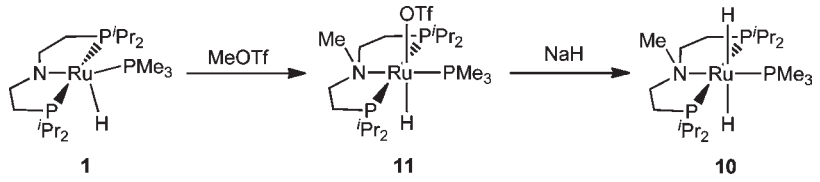

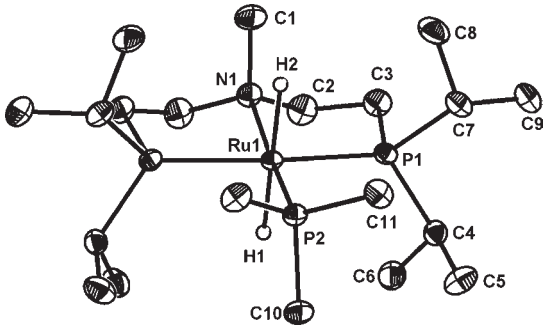

Figure 7. DIAMOND plot of **10** in the crystal with thermal ellipsoids drawn at the 50% probability level. Hydrogen atoms other than H1 and H2 are omitted for clarity. N1, Ru1, and H1 define a crystallographic mirror plane.

Table 3. Selected Bond Lengths and Bond Angles of **10** in the Crystal

bond lengths (Å)			
Ru1−P1	2.3011(4)	Ru1−N1	2.270(2)
Ru1−P1[a]	2.3011(4)	Ru1−P2	2.2373(5)
bond angles (deg)			
N1−Ru1−P1	82.29(1)	P1−Ru1−P1[a]	163.40(2)
N1−Ru1−P1[a]	82.29(1)	N1−Ru1−P2	174.32(4)
P1−Ru1−P2	97.98(1)	P1[a]−Ru1−P2	97.98(1)

[a] Symmetry operation for equivalent atoms (x, $1/2 - y$, z).

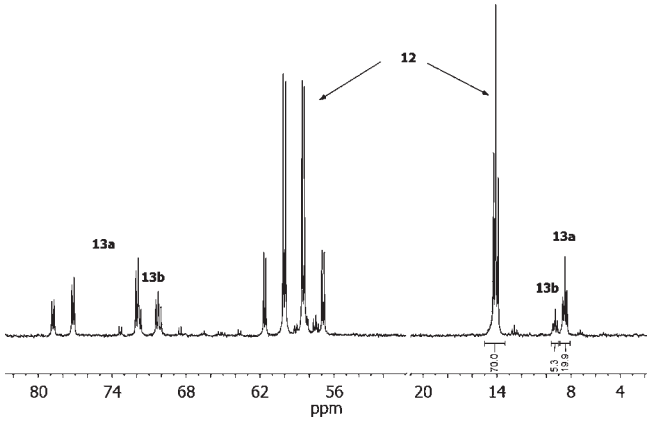

Figure 8. Representative ^{31}P NMR spectrum of the reaction of **3** with MeOTf in benzene.

Scheme 8. Reaction of Enamido Complex **3** with MeOTf

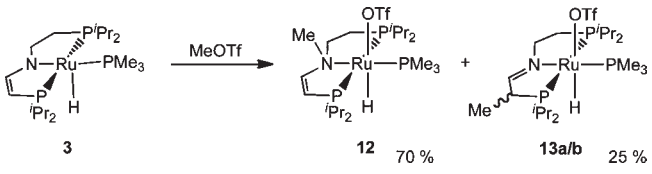

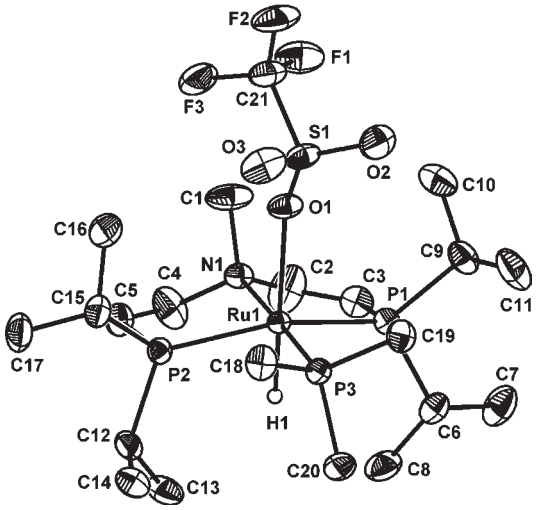

Figure 9. DIAMOND plot of **12** in the crystal with thermal ellipsoids drawn at the 50% probability level. Hydrogen atoms other than H1 are omitted for clarity.

Table 4. Selected Bond Lengths and Bond Angles of **12** in the Crystal

bond lengths (Å)			
Ru1−P1	2.3348(5)	Ru1−N1	2.249(2)
Ru1−P2	2.3194(5)	Ru1−P3	2.2579(5)
C2−C3	1.341(3)	C4−C5	1.426(3)
bond angles (deg)			
N1−Ru1−P3	178.87(4)	P1−Ru1−P2	154.31(2)
N1−Ru1−P1	82.08(4)	N1−Ru1−P2	82.71(4)
P1−Ru1−P3	98.01(2)	P2−Ru1−P3	96.81(2)

Scheme 9. Reaction of Enamido Complex **3** with PMe_3

results in *C*-methylation in 71% isolated yield, i.e., the reversed selectivity compared with **3**.[30c] As for **3**, for this aromatic analogue, the authors indicated a larger NPA charge on the γ-C than on the N atom. Therefore, the different selectivities of **3** and **A** suggest that the reaction with electrophiles is not only controlled by charge but also by kinetic arguments, such as the higher flexibility of the PNP′ ligand, which enables pyramidalization of the nitrogen atom compared with the planar pyridine based PNP ligands.

Multinuclear NMR spectroscopic data for **12** are in agreement with the structure depicted in Scheme 8, with a meridional arrangement of the *Me*PNP′ chelate ($^2J_{PP}$ = 262 Hz), a mutual *trans*-configuration of the hydride

Scheme 10. Reaction of Amido Complex **1** with PMe_3 and Proposed Mechanism

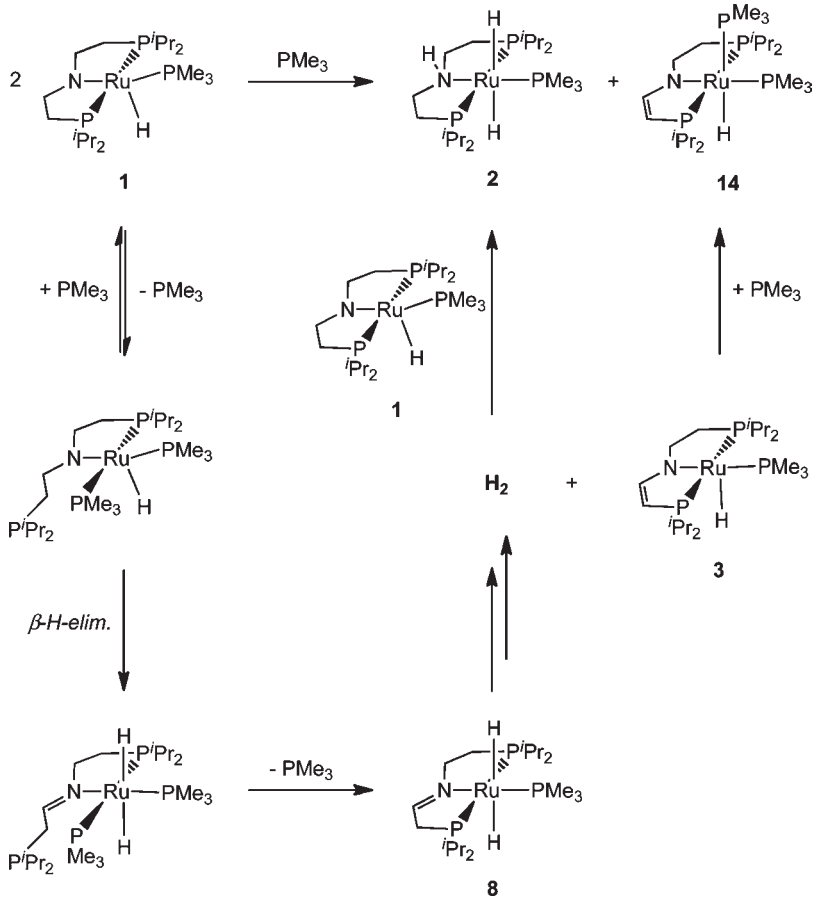

(^{1}H: −25.92 ppm) and triflate ligands, and an *N*-bound methyl group (^{1}H: 2.28 ppm). This structural assignment was confirmed by X-ray diffraction in the solid state (Figure 9 and Table 4). The triflate anion is loosely bound to the metal center (Ru−O1 2.356(1) Å). The *Me*PNP′ ligand exhibits a short C=C (C2−C3 1.341(3) Å) and a long C−C (C4−C5 1.426(3) Å) bond on the respective "arms" of the chelate backbone. However, the relatively short C4−C5 single bond length points toward some disorder in the crystal structure as observed for imine complex **7** (vide supra).

Regarding the reactivity of **3** with nucleophiles, the relatively low-lying, metal centered LUMO suggests Lewis-acidic behavior of the ruthenium atom for this complex. Therefore, this reactivity of **3** was probed by reaction with PMe_3. Accordingly, the octahedral diphosphine complex [RuH(PMe_3)$_2$(PNP′)] (**14**) is obtained in quantitative yield (Scheme 9). The $^2J_{PP}$ coupling constants of the four ^{31}P signals, the hydride chemical shift (−10.30 ppm), and the large $^2J_{HP}$ coupling constant of the hydride with a PMe_3 ligand (88 Hz) are in agreement with a meridional coordination of the PNP′ chelate and mutual *cis* arrangement of the two PMe_3 ligands.

Owing to the large HOMO−LUMO gap of amido complex **1**, a different reactivity with nucleophiles can be expected as compared with **3**. In fact, upon the addition of PMe_3 to **1**, no immediate reaction is observed, but considerable broadening of all ^{31}P NMR signals, i.e., the pincer ligand, coordinated PMe_3, and free PMe_3, respectively. Monitoring the sample by ^{31}P NMR over 2 days reveals complete conversion to an equimolar mixture of amine complex **2** and enamid **14**, but no intermediates could be detected. This result can be explained by the following proposed mechanism (Scheme 10): The broadening of the ^{31}P NMR signals indicates rapid exchange of free PMe_3 with the coordinated phosphine ligands. This exchange process could open up a pathway for β-hydride migration with lower barriers, as compared with **1** in the absence of PMe_3 (*vide ultra*), because the NCH_2 protons of a dissociated pincer "arm" could adopt a more favorable conformation in the transition state. The thermodynamic instability of resulting imine **8** toward H_2-elimination was discussed in section 1.2. Finally, eliminated H_2 adds to amide **1** and **3** is trapped by PMe_3 to give the observed mixture of **2** and **14**. This interpretation suggests that nucleophiles might generally reduce the stability of chelate stabilized late metal amides toward β-hydride migration. Most importantly, the simple change in saturation of the PNP chelate backbone strongly alters the reactivity toward nucleophiles, attributable to the change in N→Ru π-donation of the amido function.

Concluding Remarks

Cooperative behavior of the *N*-functionality in late transition metal amido complexes has been well examined and utilized, e.g., for Noyori-type hydrogenations. More recently, with pyridine-based amido pincer complexes, the chelate backbone cooperativity afforded new catalytic alcohol functionalization reactions. In this context, the present aliphatic

PNP ruthenium system offers unusual 2-fold metal−ligand cooperativity, both at the nitrogen atom and the ligand backbone. This reactivity is highly useful for easy pincer ligand functionalization and for bifunctional bond activation reactions, e.g., of H_2.

Access to backbone ethylene-bridge functionalization is provided by the formation of enamido complex **3** from **5** and KO*t*Bu. Independent synthesis suggests imine complex **7** to be an intermediate in this reaction, which is formed by β-hydride migration from **6** and undergoes reversible γ-C deprotonation toward **3**. Both amide **1** and enamide **3** exhibit distinct *N*-centered reactivity with electrophiles, e.g., MeOTf, which distinguishes **3** from similar, pyridine-based, aromatic pincer complexes, attributable to the high flexibility of the aliphatic analogon. However, while **3** reacts with PMe_3 to octahedral complex **14**, **1** gives a mixture of **2** and **14** via a β-hydride migration pathway. This considerably different reactivity of **3** versus **1** with nucleophiles nicely demonstrates the weaker π-donation by the new enamido type ligand PNP′ of **3**, as compared to amido ligand PNP, which is further expressed in their molecular structures. Therefore, with respect to electronic properties, we tend to categorize the PNP′ ligand in the series of known amido pincer ligands between the strongly basic dialkylamido PNP ligand and the disilylamido ligands $N(SiMe_2CH_2PR_2)_2$. In this context, the preparation of doubly unsaturated, anionic ligands, such as $N(CHCHPR_2)_2$, would be desirable to bridge the gap toward weakly π-donating PNP pincer ligands like the diphosphinoarylamides $N(C_6H_4PR_2)_2$.

The quantum-chemical examination of bifunctional reversible H_2 addition/elimination of enamido complex **3**, amido complex **1**, and amine complex **2** explains why imine intermediate **8** is not observed experimentally. In comparison, imine complex **7** can be isolated, attributable to the weaker *trans*-influence of the chloride ligand in **7**. Hence, the *trans*-dihydride configuration might generally stabilize Noyori-Morris-type (de)hydrogenation catalysts against deactivation to an imine complex. Experimental and theoretical results suggest β-hydride migration to the metal and proton transfer to hydride ligands with sizable barriers as the mechanism for the **3** ⇔ **1** ⇔ **8** ⇔ **2** reaction sequence. We have no evidence for predissociation of a pincer phosphine "arm" to be necessary for this process.

Acknowledgment. The authors thank the DFG (Emmy-Noether Programm: SCHN950/2-1), the Fonds der Chemischen Industrie, the Dr.-Otto-Röhm-Gedächtnisstiftung and the Dr.-Ing.-Leonhard-Lorenz-Stiftung for funding, and the Elitenetzwerk Bayern for a graduate fellowship (A.F.).

Supporting Information Available: The 2D NMR spectra of **2**, **7**, **12**, and **14** in PDF format; crystallographic information for **1**, **4**, **5**, **7**, **10**, and **12** in PDF and CIF format; coordinates for the optimized geometries of $\mathbf{2^{Me}}$, $\mathbf{TS(2^{Me}/1^{Me}\text{-}H_2)}$, $\mathbf{1^{Me}\text{-}H_2}$, $\mathbf{TS(1^{Me}\text{-}H_2/1^{Me})}$, $\mathbf{1^{Me}}$, $\mathbf{TS(1^{Me}/8^{Me})}$, $\mathbf{TS(8^{Me}/3^{Me}\text{-}H_2)}$, $\mathbf{3^{Me}\text{-}H_2}$, $\mathbf{TS(3^{Me}\text{-}H_2/3^{Me})}$, $\mathbf{3^{Me}}$, **1**, and **3** and frontier orbital diagrams of **1** and **3** in PDF format. This material is free of charge via the Internet at http://pubs.acs.org.